

Simultaneous pulse rate estimation for two individuals that share a
sensor-laden bed

by

Dong Xu Ren

B.Eng., The Australian National University, 2011

A THESIS

submitted in partial fulfillment of the requirements for the degree

MASTER OF SCIENCE

Department of Electrical & Computer Engineering
College of Engineering

KANSAS STATE UNIVERSITY
Manhattan, Kansas

2019

Approved by:

Major Professor
Steve Warren

Copyright

©2019 Dong Ren

Abstract

Sleep monitoring has received increased attention in recent years given an improved understanding of the impact of sleep quality on overall well-being. A Kansas State University team has developed a sensor-based bed that can unobtrusively track sleep quality for an individual by analyzing their ballistocardiograms (BCGs) while they lay on the bed, foregoing the need to visit a sleep clinic to quantify their sleep quality. A BCG is a signal that represents cardiac forces that have spread from the heart to the rest of the body – forces that result in part from the injection of blood into the vascular system. The sensor bed software can extract BCG-based health parameters such as heart rate and respiration rate from data acquired continuously throughout the night. Such a toolset creates a new challenge, namely that many people sleep on a shared bed. In such cases, a given sensor bed would acquire mixed BCGs that contain information for both people.

This thesis documents efforts to create an algorithm to extract individual health parameters from mixed parent BCGs obtained from bed sensors that reside on a shared bed. The first component of the two-part algorithm performs ‘blind source separation:’ a technique originally designed for mixed audio applications that attempts to optimally separate two individual BCGs contained in an original mixed signal. The second component of the algorithm utilizes a frequency-domain, peak-scoring method to identify the most likely fundamental BCG harmonic for each separated signal – a harmonic that corresponds to the pulse rate for that individual. The peak-scoring approach allows the algorithm to overcome challenges associated with different time-domain BCG waveform shapes, the presence of signal artifact, and the loss of BCG characteristic features that occurs during the separation stage. These challenges can be problematic for time-domain pulse rate algorithms, but the repetitive waveform patterns can be exploited in the frequency-spectrum.

The peak-scoring algorithm was verified by comparing pulse rates determined from single-subject BCGs (obtained in various sleeping positions) against pulse rates determined from simultaneously collected electrocardiograms. The separation and peak-scoring components were combined together, and this overall technique was applied to over 20 sets of paired BCG data, with variations in sensor placement, sensor type and mattress type. Early results indicate the ability of the algorithm to determine pulse rates from mixed BCGs with acceptable levels of success but with areas for improvement.

Table of Contents

List of Figures	vi
List of Tables	ix
Acknowledgements	x
Chapter 1 - Introduction.....	1
1.1. Sleep Monitoring and the Importance of Sleep Quality	1
1.2. Bed-Based Instrumentation.....	1
1.2.1. Two-Body Problem.....	2
1.3. The Ballistocardiogram.....	3
1.4. Heart Rate Estimation	5
1.5. Signal Separation	6
Chapter 2 - Literature Review.....	9
2.1. Sleep Monitoring at Home.....	9
2.2. Heart Rate Estimation Techniques	10
2.2.1 Beat-to-Beat Detection.....	10
2.2.2. Template Matching Approach	11
2.2.3. Cepstrum Method.....	11
2.3. Blind Source Separation in Biomedical Applications	12
2.3.1. Independent Component Analysis	12
2.3.2. Joint-Approximation Diagonalization of Eigenmatrices	13
Chapter 3 - The Ballistocardiogram and the Experimental Sensor-Bed System	15
3.1. The Ballistocardiogram.....	15
3.1.1. BCG Waveform Description.....	16
3.2. Bed Setup and BCG Acquisition	17
3.2.1. Bed and Film Setup.....	17
3.2.1. BCG Acquisition.....	19
3.2.3. Signal Processing	20
3.3. Two-Body Problem.....	21
3.3.1. Film and Load Cell Setup	23
3.3.2. Pulse Rate Determination.....	24

Chapter 4 - Pulse Rate Estimation Method.....	26
4.1. Peak Scoring Algorithm.....	26
4.1.1. BCG Frequency Domain Spectra.....	27
4.1.2. Algorithm Ranking Technique	28
Chapter 5 - Two Body Problem.....	38
5.1. Two-person BCG Frequency Domain Spectrum.....	38
5.2. Signal Separation Applied to Mixed BCGs.....	39
5.2.1. Independent Component Analysis	40
5.2.2. Multidimensional Independent Component Analysis.....	40
Chapter 6 - Results and Performance.....	49
6.1. Acquired BCG Recordings	49
6.2. Estimated Pulse Rates Using the Peak-Scoring Algorithm	49
6.2.1. Films Versus Load Cells.....	51
6.2.2. Effects of Sleeping Position.....	56
6.2.3. Effects of Mattress Type.....	59
6.2.4. Effects of Motion Artifact.....	61
6.3. Mixed BCGs	62
6.3.1. Films Versus Load Cells.....	64
6.3.2. Effects of Film Placement.....	66
6.3.3. Effects of Mattress Type.....	68
6.4. Performance Summary	70
Chapter 7 - Conclusion	71
7.1. Future Work.....	71
References	73
Appendix A - Separation Data Results.....	78

List of Figures

Figure 1. Two head-to-foot BCG cycles acquired with an EMFi, where the subject is sleeping in a supine position.	4
Figure 2. ECG R-peak identification and R-R interval determination resulting from the application of the Pan-Tompkins algorithm.	5
Figure 3. Time-aligned ECG and BCG waveforms.	16
Figure 4. BCG waveforms acquired with EMFis for common sleeping positions: (top left) supine, (top right) right side, (bottom left) left side, and (bottom right) prone.	17
Figure 5. EMFi and load cell configuration on the sensor bed.	18
Figure 6. Two types of sensors employed by the sensor bed: (left) EMFis arranged in a 4 x 1 array underneath the mattress, and (right) load cell to be placed under each bedpost.	19
Figure 7. Frequency spectra of unfiltered BCGs recorded using an EMFi (left) and a load cell (right). The respiration component is prominent in the spectrum from the EMFi.	20
Figure 8. Unfiltered and filtered EMFi BCG segments.	21
Figure 9. A three-second segment of a mixed BCG, recorded using an EMFi, for two subjects lying in supine positions on a shared bed. From the plot, there are no distinct features which could be used to visually identify the pulse rate of each individual.	22
Figure 10. EMFi placement configurations: (left) all four EMFi films placed directly below one subject, and (right) two films placed directly under each subject.	24
Figure 11. Flow diagram detailing the process of estimating pulse rate from mixed BCGs.	25
Figure 12. BCG frequency spectra of 60-second segments acquired for various sleeping positions: (top left) supine, (top right) right side, (bottom left) left side, and (bottom right) prone. Sleeping position affects the strongest harmonic in the frequency spectrum.	27
Figure 13. Spectrum of a 60-second film-based BCG segment with the identified peaks numbered. The prominent peak (#21) is the 4 th harmonic.	30
Figure 14. Overall process associated with the peak-scoring algorithm.	35
Figure 15. BCG segments collected from each of the four films during the same time interval as in Table 2. Minor subject movement appears just before the 5-second mark, but only the BCGs from films 0 & 1 were affected in a major way.	36

Figure 16. Frequency spectrum of a mixed BCG, where each of the two individuals is lying on the bed in a supine position.....	39
Figure 17. Mixed BCGs gathered from four EMFis when two people lie on the bed.....	43
Figure 18. Estimated signals, \mathcal{S} , using the estimated separation matrix, $\mathbf{A} - \mathbf{1}$, produced by running the JADE algorithm.	44
Figure 19. Separated signals acquired from all four films (subject A).	47
Figure 20. Frequency spectrum of a one-minute segment of separated signal 1 in Figure 19. A harmonic is visible at peak 5.....	47
Figure 21. Separated signals acquired from all four films (subject B).	48
Figure 22. Frequency spectrum of a one-minute segment of separated signal 1 in Figure 21. A distinct harmonic is visible at peak 2.	48
Figure 23. Bland-Altman plot comparing estimated pulse rates from BCGs to pulse rates from ECGs for both film and load cell sensors.	50
Figure 24. BCG recordings from EMFis and load cells for a single person on the bed. Slight differences in waveform patterns are apparent between the two sensor types.	52
Figure 25. Respiration harmonic mistaken for a pulse rate fundamental harmonic: (left) an unfiltered BCG spectrum that includes a respiration harmonic at 0.25 Hz with harmonics at 0.5 and 1.0 Hz, respectively, and (right) a filtered spectrum with the fundamental respiration harmonic removed.	54
Figure 26. Bland-Altman plot comparing estimated BCG and ECG pulse rates using data acquired with films, where film data are affected by respiration harmonics.....	55
Figure 27. Bland-Altman plot comparing estimated BCG and ECG pulse rates using data acquired with films, where film data are not affected by respiration harmonics.....	55
Figure 28. Bland-Altman comparing estimated BCG results and ECG results using data measured from load cells.	56
Figure 29. Bland-Altman plot comparing pulse rates estimated from BCGs and ECGs for a single subject sleeping in a supine position.....	57
Figure 30. Bland-Altman plot comparing pulse rates estimated from BCGs and ECGs for a single subject sleeping on their right side.....	58
Figure 31. Bland-Altman plot comparing pulse rates estimated from BCGs and ECGs for a single subject sleeping on their left side.....	58

Figure 32. Bland-Altman plot comparing pulse rates estimated from BCGs and ECGs for a single subject sleeping in a prone position.	59
Figure 33. Bland-Altman plot comparing pulse rates estimated from BCGs and ECGs for a single subject sleeping on a soft mattress.	60
Figure 34. Bland-Altman plot comparing pulse rates estimated from BCGs and ECGs for a single subject sleeping on a hard mattress.	61
Figure 35. BCG with minor motion artifact (left), which carries over to the frequency spectrum (right).	62
Figure 36. BCG mixture separated into two separate BCGs.	63
Figure 37. Mixed BCG collected from an EMFi and separated into two BCG source components using MICA decomposition.	64
Figure 38. Box-plot for pulse rate comparisons given different sensor types.	65
Figure 39. Box plot for pulse rate comparisons given different film configurations.	67
Figure 40. Box plot for pulse rate comparisons given different mattress types.	69

List of Tables

Table 1. Example peak scoring and ranking for the spectrum in Figure 13.	34
Table 2. Estimated pulse rates for four 1-minute BCG segments from four EMFis for a subject lying in a supine position.	36
Table 3. Estimated pulse rates after applying the peak-scoring algorithm to the estimated signals, S	45
Table 4. RMS errors for the pulse rates determined from film and load cell BCGs.	53
Table 5. Pulse rate error as a function of sleeping position.	57
Table 6. RMS pulse rate errors for various mattress/sensor combinations.	60
Table 7. RMS errors for pulse rates determined from EMFi and load cell BCGs for the two- subject study.	65
Table 8. RMS errors for pulse rates obtained using different film configurations in the two- person study.	66
Table 9. RMS errors for pulse rates obtained from BCGs using different mattress types (two- person study).	68
Table 10. Single subject, Soft Mattress, Film sensors	78
Table 11. Single subject, Soft Mattress, Load cell sensors	79
Table 12. Single subject, Hard Mattress, Film sensors	80
Table 13. Single subject, Hard Mattress, Load cell sensors	81
Table 14. Soft Mattress, Film, Config 1	82
Table 15. Soft mattress, Load Cell, Config 1	82
Table 16. Soft Mattress, Film, Config 2	83
Table 17. Soft Mattress, Load Cell, Config 2	83
Table 18. Hard Mattress, Film, Config 1	84
Table 19. Hard Mattress, Load Cell, Config 1	84
Table 20. Hard Mattress, Film, Config. 2	85
Table 21. Hard Mattress, Load Cell, Config. 2	85

Acknowledgements

I would like to thank my major professor, Dr. Steve Warren, for his guidance, wisdom and patience. My appreciation also goes out to my committee members, Dr. Dave Thompson, Dr. Bala Natarajan, and Dr. Punit Prakash for their continued support and guidance throughout my graduate career. I wish to show my gratitude to the Department of Electrical & Computer Engineering (ECE) and the KSU College of Engineering for providing me with the opportunity to pursue my graduate studies. The opportunity to work with these wonderful people in an amazing environment is beyond my expectation. I also wish to acknowledge the ECE staff for all of their assistance and support. This work would not have been possible without them.

I wish to show my appreciation to Dr. Carl Ade for providing a private location at KSU Lafene Health Center to conduct our studies without interruption.

I would like to acknowledge and thank the team in the Medical Component Design Laboratory for their assistance and support over the duration of the research, especially Charles Carlson, who has acted as a second mentor.

Lastly, I would like to thank my family for their support and encouragement, and especially my fiancée, Beibei Li, for being by my side through my graduate career.

Chapter 1 - Introduction

1.1. Sleep Monitoring and the Importance of Sleep Quality

Sleep quality is important for an individual's health and well-being, with the average person spending about one-third of their life sleeping or attempting to do so [1]. Strong evidence links poor quality of sleep with poor health and well-being, and poor sleep can contribute to increased workplace stress. Traditionally, a polysomnograph (PSG) is used to monitor sleep quality, where the technique records a collection of biometric measurements throughout the night, including electrooculograms (EOGs), electrocardiograms (ECGs), electromyograms (EMGs), and respiration rates. While the PSG has been accepted as the 'gold' standard for sleep assessment, other sleep quality platforms have recently emerged, such as wearable sleep trackers [18]. The invasive nature of wires and electrodes attached physically to the body, and/or the need to wear a device while sleeping, can cause discomfort and render PSGs and wearable sleep trackers unusable, especially for more vulnerable populations such as the elderly or children with severe disabilities [3]. For this reason, non-invasive monitoring and sleep quality assessment have been receiving increased attention.

1.2. Bed-Based Instrumentation

Ballistocardiography is an attractive means to accomplish non-invasive sleep monitoring due to (a) the ease of integrating the affiliated sensors into a bed or mattress and (b) the ability to obtain a ballistocardiogram (BCG) from a subject without their knowledge of the presence of these sensors. These sensors neither cause discomfort nor interfere with the subject's regular sleep behavior, and they can be easily installed and readily hidden within the bed system. Many methods exist to record BCGs unobtrusively, including pressure sensors within an air-mattress [4], force sensors [5], load cells installed under bed posts [6], polyvinylidene fluoride (PVDF) film sensors [44], strain gauges [45], and electromechanical film (EMFi) sensors either above or beneath a mattress. These sleep monitoring setups are non-invasive, and they require no patient compliance or interaction, making them well suited for the general population.

A bed-based instrumentation system for unobtrusive sleep quality assessment was developed by Carlson *et al.* at Kansas State University [2]. The system utilizes an array of four electromechanical films (EMFis) placed under the mattress and four load cells installed under the bed posts to non-invasively acquire BCGs from the subject while they lay on the bed – BCGs from which information such as heart rate and respiration rate can be obtained. This bed-based instrumentation is being utilized at Heartspring, Wichita, KS, for the assessment of sleep quality in severely disabled children, with a goal to find relationships between nighttime well-being and daytime wellness and behavior. Nearly all of these children have low-functioning autism, and it is vitally important that such instrumentation be hidden in a bed so that a given child is unaware of its presence. *Chapter 3* outlines the sensor bed instrumentation setup in more detail, since this setup forms the core of the instrumentation utilized to study the two-body problem that is the focus of this thesis.

1.2.1. Two-Body Problem

The notion of bed-based, non-invasive BCG measurements during sleep can be applied in a common household, meaning sleep quality assessment without the need to visit a sleep clinic and sleep in an unfamiliar bed. This environment, however, introduces another challenge, which is that many people share a bed with another individual when sleeping at night. For the purposes of this research, the sensor-bed setup by Carlson *et al.* was modified to a full-size bed that accommodates two people at the same time. As a result, a BCG recorded by a given EMFi sensor or load cell will be a mixed signal comprised of the BCGs from both users coupled with mattress- and motion-induced artifacts. To extract the heart rate and respiration rate information for the person of interest, a mixed signal needs to be processed to either directly extract the BCG of interest (with the rest of the mixed signal dismissed as noise) or perform source separation on the mixed signal, which means separating the individual BCGs to extract the heart rate information for *both* subjects. The waveform characteristics of a mixed BCG differ greatly from those of a single-subject BCG, so traditional methods of heart rate and respiration rate extraction from single-subject BCGs cannot be applied to these mixed BCG recordings.

1.3. The Ballistocardiogram

Ballistocardiography is the measurement of ballistic forces on the body in response to the cardiac ejection of blood into the vascular system [3]. During each heartbeat, the blood traveling through the vascular system causes a change in the body's center of mass. The body recoils slightly to maintain balance, and the related forces can be quantified in the form of a BCG. The BCG was first observed and recorded in 1877 by Gordon, who noticed that while a subject was standing on a weighing scale, the needle would oscillate in sync with the subject's heartbeat [15]. This concept was not revisited again until 1936, when Starr *et al.* [40] created an instrument which allowed repeatable measurement of these ballistic forces. In the past two decades, the popularity of BCGs has increased given renewed clinical interest in unobtrusive cardiac assessments. A number of methods to obtain BCGs are discussed in [3]: they are measured in terms of displacement, velocity, and acceleration, and these forces travel in all axial directions. The bed-based instrument utilized in [2] collects dorso-ventral BCGs, but can also collect longitudinal BCGs, which are the strongest of these projected 3D forces upon the body.

Applied force on an electromechanical film (EMFi), for example, will result in a change in voltage across the film's contacts: voltage that when tracked versus time can form a signal commensurate with the applied force. A typical BCG segment for a subject sleeping in a supine position, as measured using an EMFi film, is depicted in Figure 1. This BCG waveform contains several labeled peaks, where the most noticeable peak within a given BCG cycle is the J peak within the IJK complex. This complex, similar to a QRS complex in an ECG, is associated with systole [20]: the contraction of the ventricles that moves blood into the arteries. The amplitude of the J peak fluctuates in cyclical synchrony with respiration.

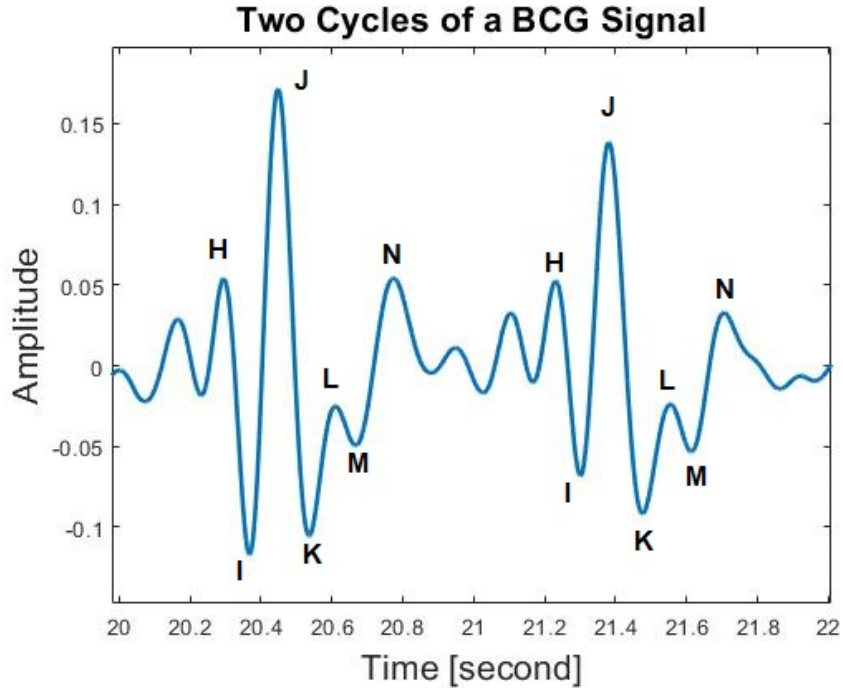


Figure 1. Two head-to-foot BCG cycles acquired with an EMFi, where the subject is sleeping in a supine position.

While there can be many variations of BCGs, the structure of each cycle within an overall signal is similar, though minor differences can occur in the waves following each IJK complex. These follow-on waves are not always seen as a representation of the BCG itself but rather can reflect artifact due to the aperiodic heartbeat, meaning constructive and destructive interference between the current and previous heartbeat signal components [20]. In other words, such interference occurs because the duration of a typical BCG pulse is longer than a typical heartbeat interval. Due to the numerous methods by which BCG recordings can be obtained, plus the various 3D directions of the ballistic forces, the shape of a BCG waveform can vary greatly, so specifying the direction of a measurement and the position/type of the sensor is important. Further, a person's numerous sleeping positions and orientations provide different directions for BCG force projections. For the purpose of this work, only the most common sleeping positions were observed.

1.4. Heart Rate Estimation

Heart rate is a vital health parameter used to determine health and well-being. In an electrode-based setup, heart rate is commonly determined by computing the time between R peaks and then converting that R-R interval to heart rate in beats per minute (bpm). ECG waveforms are favored for heartbeat interval (HBI) applications due to the distinct and sharp QRS complexes present in these waveforms – features which are easy to distinguish and detect. Many popular algorithms have been developed to achieve this goal. One common and widely accepted method is the Pan-Tompkins algorithm [10], which utilizes both peak detection and hypothesis testing to determine the location of each R peak, as illustrated in Figure 2. The resulting R-R intervals can be determined by calculating the time between respective peaks. The information provided from R-R intervals is valuable, yielding both heart rate and heart rate variability, i.e., the variation in heart rate over a period of time [51][52]. These parameters allow for the detection of abnormal heart rhythms, or arrhythmias, which can result from a variety of chronic conditions [52][53].

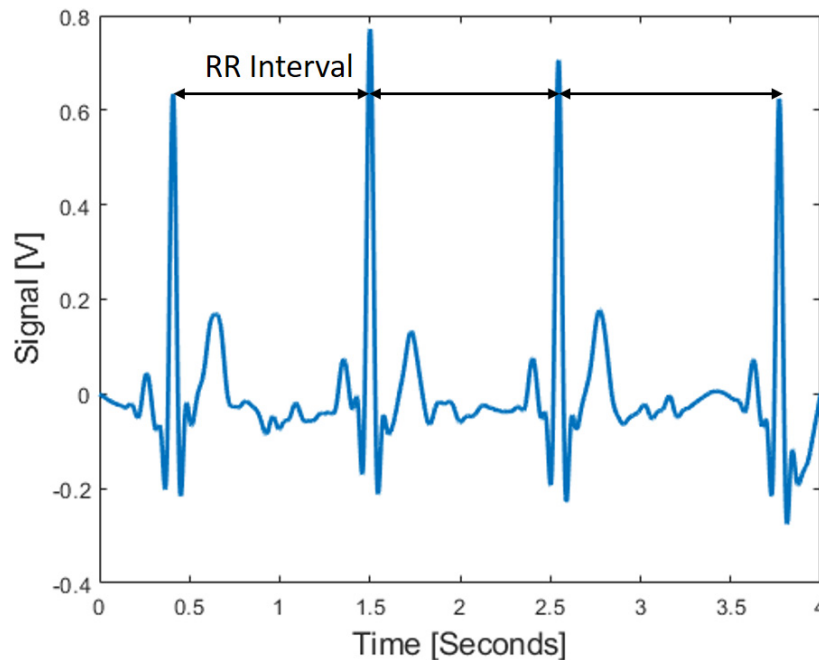


Figure 2. ECG R-peak identification and R-R interval determination resulting from the application of the Pan-Tompkins algorithm.

Unfortunately, electrodes and their accompanying wires are intrusive and render ECGs impractical for long-term sleep monitoring, despite the ease with which these signals can be processed and the wealth of information they contain. BCGs, on the other hand, are signals that result from cardiac mechanical activity and can therefore be acquired without the use of electrodes. With the acquisition of BCGs from bed sensors, accurate extraction of heart rate and respiration rate allow sensible healthcare monitoring and assessment during the night. While conventional methods for extracting such health parameters from ECGs have been studied in detail, challenges associated with parameter extraction from BCGs have not been fully explored. Many such methods have been introduced, including peak-detection algorithms that seek to identify J peaks [21], in a similar way that the Pan-Tompkins algorithm detects ECG R peaks. Due to the increased cycle-to-cycle variation in BCG morphology, J peaks are not as distinctive within a BCG waveform compared to their R-peak counterparts, so peak-detection algorithms must be carefully selected. Other BCG peak-detection methods employ template matching [22], adaptive beat-to-beat estimation [11], wavelet transformations [33], the use of the cepstrum method within the frequency domain [23], and the identification of the dominant third harmonic within the spectrum [24]. The last two methods take advantage of the frequency spectrum, and these BCG frequency components can be further explored to obtain and verify the spectral pulse rate component. One challenge lies in assuming that the subject maintains the same pulse rate throughout the analysis segment.

1.5. Signal Separation

While the bed-based instrumentation has proven useful for obtaining BCG data while a single subject lays on the bed, the feasibility of utilizing similar technology for two subjects that both lay on the bed remains to be seen. One possible approach to this problem is the use of Blind Source Separation (BSS) to split the composite BCG data into two self-consistent data streams, each of which represents a BCG for a single subject. BSS seeks to retrieve N original unknown signal sources, $s_1(t), \dots, s_N(t)$, given only the observed mixtures of those sources, $x_1(t), \dots, x_M(t)$, from M sensors, each containing a different combination of the source signals. The term ‘blind’ indicates that no prior knowledge of the original source signals exists, and no information is available regarding the mixing process. Different forms of BSS have been devised for various processing applications in fields such as communication, audio processing, and biomedical signal analysis.

Source separation is widely used in speech and audio recognition and is inspired by the popular ‘Cocktail Party Problem,’ where a listener seeks to distinguish speech from a single speaker in a room full of an arbitrary number of simultaneous speakers. A mathematical model of the ‘mixing process’ purports to determine the relationship between the source signals and the observations. The mixing process models can be classified as follows [19]:

1. ***Non-Linear Model.*** This is the most general model.
2. ***Post Non-Linear Model.*** The mixing approach is divided into two steps: linear mixing followed by instantaneous linear mapping.
3. ***Linear Model.*** The most widely studied model and the model considered in this thesis. The mapping is linear, and the linear mixing is split into two categories:
 - *Linear Convolutional Mixing.* The mixing process is a multidimensional convolution of the sources.
 - *Linear Instantaneous Mixing.* The outputs are a metrical combination of the inputs at the same time.

Convolutional linear mixing can be modeled by an impulse response, $\mathbf{h}(t)$, which connects the inputs and outputs:

$$\mathbf{x}(t) = \int \mathbf{h}(t - \tau)\mathbf{s}(\tau)d\tau. \quad (1.1)$$

Another type of simple mixing model can be defined as a linear combination of source signals at any given time, t . This model assumes mutual independence between source signals, $s_1(t), \dots, s_N(t)$, and the relationship can be modeled as

$$\mathbf{x}(t) = \mathbf{A}\mathbf{s}(t), \quad (1.2)$$

where $\mathbf{s}(t) = [s_1(t), \dots, s_N(t)]^T$ is an $N \times 1$ column vector containing the source signals, $\mathbf{x}(t) = [x_1(t), \dots, x_M(t)]^T$ is an $M \times 1$ vector containing the mixtures observed by each of the M different sensors (i.e., the sensor output signals, where $M \geq N$), and matrix \mathbf{A} is a ‘mixing matrix’ containing the mixing parameters. To reconstruct the source signals, $\mathbf{s}(t)$, given the observations,

$\mathbf{x}(t)$, an estimate of the mixing matrix, \mathbf{A} , must be found. The inverse or pseudo-inverse, \mathbf{Q} , is then determined, such that $\mathbf{Q} = \mathbf{A}^\#$, where $\#$ denotes a Moore-Penrose pseudo-inverse. \mathbf{Q} is known as the ‘separation matrix,’ which is used in conjunction with $\mathbf{x}(t)$ to determine $\mathbf{s}(t)$:

$$\mathbf{s}(t) = \mathbf{Q}\mathbf{x}(t). \quad (1.3)$$

While BSS has been widely utilized for the separation of biometric parameters, many challenges still remain when utilizing BSS for the separation of mixed bed-based BCGs. Some differences between BCGs and audio signals follow:

- The range for male/female voice fundamental frequencies is approximately 120 Hz to 210 Hz [17]. Fundamental pulse rates at rest exist in the range of 0.5 Hz to 2 Hz [47].
- While it is uncommon for two people to share fundamental voice frequencies in speech, it is not unusual for two people to have similar pulse rates.
- Audio sources are reasonably considered to be mutually independent and propagate in air, whereas ballistic forces from heartbeats propagate through a shared mattress and cannot be assumed to be mutually independent.

Despite these challenges, bed-based BCG mixed signals are linearly mixed similar to mixed speech signals, implying that suitable BSS algorithms can be applied to these BCGs.

For this effort, the instrumentation sensor bed developed in [2] was modified to be suitable for two-person studies so as to gather mixed BCGs from two individuals simultaneously lying on the bed. *Chapter 2* discusses existing methods for (a) heart rate estimation from BCGs and (b) separation of mixed signals. Time- and frequency-domain differences between single-person BCGs and two-person mixed BCGs measured using the sensor bed are described in *Chapter 3*. *Chapter 4* looks at how a frequency-based, peak-scoring algorithm can be used to estimate pulse rate for a single-subject BCG, and *Chapter 5* explains how source separation algorithms used for speech processing can be utilized to separate mixed BCGs into their source components. The performance of the separation and peak-scoring algorithms are described in *Chapter 6*.

Chapter 2 - Literature Review

This chapter explores literature in the fields of at-home sleep monitoring and non-invasive BCG acquisition. It also seeks to analyze various heart rate estimation techniques employed with BCGs along with signal separation methods commonly used for biomedical applications. Challenges associated with BCGs are highlighted, driven by their differences when compared to other types of biomedical signals.

2.1. Sleep Monitoring at Home

A number of systems have been proposed for home use, which allow non-invasive acquisition of physiological data during sleep. These devices track sleep quality by measuring parameters such as heart rate, movement during sleep, snoring, and temperature. Sleep-tracker products currently on the market include wearable trackers such as Fitbits [26], Oura Rings [27] and Polar heart rate monitors [28]. The FitBit and Oura Ring products, for example, utilize photoplethysmography to measure pulse rate and accelerometry/gyrometry to monitor movement. They are worn on the wrist and finger, respectively. These sleep monitoring devices do not provide respiration information and must be worn at all times, which can lead to inconvenience, discomfort, and a lack of patient compliance. Sleep monitoring can also take on the form of non-contact monitoring, e.g., using wireless radar as in the system developed by Adib *et al.* [29], which emits a radar burst and tracks the time for the burst to return to the transceiver. Pulsing the radar at a rapid rate allows the reflected bursts to track changes in chest movement during respiration as well as chest vibrations resulting from each heartbeat. Liu *et al.* utilized fine-grained channel information, or Channel State Information (CSI), from existing WiFi network to track body movements. These non-contact systems involve integrating sensors and their support resources into the bedroom.

Non-contact, bed-based sensor systems that acquire BCG data have gained popularity in recent years [49][50]. Variations on this approach rely on similar signal and data-acquisition principles, where sensors integrated into the bed itself (e.g., coupled to the mattress or to the bed frame) measure subject BCGs as they sleep without interfering with regular sleep behavior.

2.2. Heart Rate Estimation Techniques

Heart rate and pulse rate are traditionally estimated using an electrocardiogram (ECG) or photoplethysmogram (PPG), respectively. While algorithms for BCG-based pulse rate estimation exist, none of these approaches can be considered a ‘gold standard.’ When compared to an ECG, a BCG has more cycle-to-cycle variability, it can contain oscillations due to the spring-mass response of a mattress, and its signal-to-noise ratio (SNR) may be poor, rendering some traditional peak-detection methods ineffective. A BCG is a measurement of the mechanical activity of the heart, and the waveform can vary in shape and content as it moves through the subject and the bed medium, resulting in heartbeat interval (HBI) timing differences when compared to an ECG. The different sleeping positions taken by a subject, coupled with the many directions of force relative to the body axis, further contribute to the overall BCG shape. Therefore, a BCG waveform may not contain, e.g., a distinct J peak consistent with a corresponding ECG’s distinct R-peak. This causes difficulties in peak-detection algorithms designed to find peak locations and calculate the intervals between those J peaks (i.e., HBIs) toward the determination of heart rate variability (HRV).

2.2.1 Beat-to-Beat Detection

Despite the challenges, attempts have been made to implement BCG peak-detection algorithms to determine HRV, which can yield information about arrhythmias and sleep states [51-53]. Several methods for BCG beat-to-beat detection have been implemented, three of which were reviewed by Suliman *et al.* [32], and the algorithm by Bruser *et al.* [11] was determined to be the best performing algorithm. Bruser’s “beat-to-beat estimation by adaptive training” (BEAT) algorithm extracts a short segment of the processed BCG data to use in a ‘training phase,’ and the remaining signal is analyzed for heart beats using the features found in the training segment. A set of estimated heart beat locations is used to generate a set of refined beat-to-beat intervals. Whenever the BCG shape changes, e.g., due to a change in sleeping position, the training phase is repeated to help the algorithm adapt to the changed pattern. While this algorithm provides the least error of the algorithms reviewed, as determined by the fewest *false positives* and *false negatives*, the algorithm can still be unreliable. It also takes, on average, approximately 5 seconds to run for a one-minute BCG segment and is computationally expensive.

2.2.2. Template Matching Approach

The template matching approach to identifying BCG J-peak locations relies on finding the correlation between a previously defined ‘template signal’ and the remaining BCG. This approach is similar to Bruser’s adaptive beat estimation technique mentioned above, but instead of extracting waveform features from the template, the template-matching algorithm looks at the correlation coefficient between the extracted template and the remaining signal as a function of time, i.e., using a sliding window. Shin *et al.* proposed this technique in [22], utilizing a correlation coefficient, $r_{X,Y}$, defined as

$$r_{X,Y} = \frac{\text{cov}(X, Y)}{\sigma_X \sigma_Y} \quad (2.1)$$

where X is the template signal, Y is the BCG, $\text{cov}()$ indicates the covariance, and σ_X and σ_Y are the standard deviation of X and Y , respectively.

After the BCG is processed to remove respiration and other unwanted artifacts, at least 10 individual BCG cycles are selected, and the ensemble average of these cycles is calculated after aligning these cycles based on their J-peak locations. A moving-window operation is performed, which produces the correlation coefficient between the constructed template (the ensemble-averaged segment) and the BCG using Equation 2.1. During this sliding-window operation, when the BCG cycle in the template better ‘matches’ a corresponding BCG section, $r_{X,Y}$ increases, indicating strong correlation. By observing the incidents of high $r_{X,Y}$ peaks, the locations of the J peaks can be determined in the BCG. While this approach has displayed promising results given preliminary data, its main disadvantage involves the requirement that a distinct J peak be present in the waveform (i.e., both in the template and the remaining signal). The algorithm also struggles when the shape of the BCG changes over time, usually as a result of a change in sleeping position.

2.2.3. Cepstrum Method

The cepstrum method utilizes the frequency-domain representation of the BCG, unlike the peak detection methods, which operate in the time domain. This method takes advantage of the repetitive, pseudo-periodic structure of the BCG, where the fundamental period is manifested as a

first harmonic in the frequency domain. The cepstrum, C_x , is defined as the inverse Fourier Transform of the logarithm of the spectrum, S_x :

$$S_x = \mathcal{F}\{x\} \quad (2.2)$$

and

$$C_x = \text{real}\{\mathcal{F}^{-1}\{\log_e(|S_x|)\}\} \quad (2.3)$$

The cepstrum is used to characterize echoes and to find pitches in human speech or audio. This method is utilized by Kortelainen *et al.* [23] to estimate sleep staging by observing a subject's HBIs using BCGs collected with EMFit sensor foils placed in between two foam mattresses. The peaks in S_x will be partially composed of secondary harmonics related to the fundamental pulse rate harmonic. The periodicity of these harmonics will correspond to a peak in the cepstral domain, which represents the 'time' or 'lag' between the harmonics in the frequency domain. Kortelainen *et al.* utilized a new cepstrum method by estimating multiple spectra using different length windows, where a final spectrum is estimated based on these multiple spectra. The cepstrum method is more robust than its previous implementation but at the cost of more complex processing.

2.3. Blind Source Separation in Biomedical Applications

Blind source separation (BSS) has been considerably successful for audio and speech processing applications, and it has been applied in biomedical contexts, including the separation of fetal and maternal ECGs [42], the extraction and removal of EMG and BCG artifacts from electroencephalograms (EEGs) [34], and the elimination of muscle crosstalk from surface EMGs [14]. It would be difficult to test all of the available BSS approaches for this BCG separation application, so a few of the more popular algorithms were selected and evaluated based on previous success when applied to relevant signal separation applications.

2.3.1. Independent Component Analysis

One of the most common BSS approaches is independent component analysis (ICA) [9, 39], a term often confused with blind source separation. ICA assumes complete independence between the source signals and assumes that all source samples are independent and identically

distributed (i.i.d). ICA attempts to estimate the ‘separation matrix,’ \mathbf{Q} , in Equation 1.3, based on the *central limit theorem*, which states that the linear combination of independent, non-Gaussian random variables has a more Gaussian distribution than the distribution of either individual variable. This means the mixed BCG observations, $\mathbf{x}(t)$, are more Gaussian than the original BCG sources, $\mathbf{s}(t)$, so source separation can be based on minimization of the Gaussianity of the reconstructed sources, $\mathbf{y}(t)$. Different methods exist to measure Gaussianity, the most common being the maximum likelihood (ML) estimation approach, which involves the log-likelihood function:

$$\log(L) = \sum_{i=1}^T \sum_{i=1}^N \log \left(f_i(\mathbf{q}_i^T \mathbf{x}(t)) \right) + T \log |\det(\mathbf{Q})|, \quad (2.4)$$

where T is the number of discrete samples within time t , N is the number of independent components, $f_i()$ is the probability density function of the i^{th} source signal, and the separation matrix, \mathbf{Q} , is expressed as $\mathbf{Q} = [\mathbf{q}_1, \dots, \mathbf{q}_N]^T$.

One common biomedical ICA application is the previously mentioned separation of fetal ECG and maternal ECG given a mixed ECG acquired at the abdomen of the mother (e.g., see Jung *et al.* [42]). The greatest drawback of ICA when considering this mixed BCG application is that ICA requires sources to be independent. As mentioned in *Chapter 1*, this requirement cannot be strictly fulfilled because of the presence of the shared mattress. The ballistic forces generated by the users’ hearts propagate through the same physical shared mattress, so each acquired BCG is a signal mixture with dependent components. ICA does, however, provide the structure for other dependent component analyses which forego the source independence requirement.

2.3.2. Joint-Approximation Diagonalization of Eigenmatrices

The joint-approximation diagonalization of eigenmatrices (JADE) algorithm is a form of BSS developed by Cardoso & Souloumiac [38] which attempts to extract independent, non-Gaussian sources from signal mixtures based on the fourth-order cumulants array obtained from the signal. Cumulants are calculated from the whitened matrix, \mathbf{Z} , where $\mathbf{Z} = \mathbf{W}\mathbf{x}(t)$, \mathbf{W} is the whitening matrix, and $\mathbf{x}(t)$ contains the observations. A cumulant array, or cumulant tensor, is a four-dimensional array where the entries are specified by fourth-order cumulants of the data:

$$\begin{aligned} \kappa_4\{x_i, x_j, x_k, x_l\} = & E[x_i x_j x_k x_l] - E[x_i x_j]E[x_k x_l] \\ & - E[x_i x_k]E[x_j x_l] - E[x_i x_l]E[x_j x_k], \end{aligned} \quad (2.5)$$

where $x_{i,j,k,l}$ represents vectors within \mathbf{Z} , and $E[]$ is the expected value of various combinations of these vectors.

For each observation, both the auto-cumulant and the cross-cumulant are determined and placed in a fourth-order array, \mathbf{K} , of dimension $n \times n \times n \times n$, where n is the number of independent sources. The fourth-order array, \mathbf{K} , is decomposed into a set of $n(n+1)/2$ symmetrical orthogonal eigenmatrices, \mathbf{M}_i , of dimension $n \times n$ using a generalization of the eigenvalue decomposition of the covariance matrix. This is done by creating a set of $n(n+1)/2$ symmetrical orthogonal matrices and projecting the cumulant arrays onto these planes such that

- n of them contain zeros everywhere except for one element of the diagonal, which equals 1, and
- the remaining matrices contain zeroes everywhere except for two elements, which are situated symmetrically with respect to the diagonal and equal $\sqrt{0.5}$.

The eigenmatrices, \mathbf{M}_i , are diagonalized based on the Jacobi algorithm, which aims to minimize the sum of the squares of the off-diagonal elements, which correspond to the fourth-order cumulants between different signals. Orthogonal diagonal eigenmatrices, \mathbf{M}_i^* , are obtained. A rotation matrix, \mathbf{V} , is responsible for the transformation between \mathbf{M}_i and \mathbf{M}_i^* , and a whitening matrix, \mathbf{W} , is projected onto this space such that $\mathbf{W}^T \mathbf{V}^T$ will result in the demixing matrix, \mathbf{Q} .

While JADE suffers from the same limitation as ICA in that the sources need to be independent, JADE is also utilized as part of another dependent component analysis discussed later in *Chapter 5*.

Chapter 3 - The Ballistocardiogram and the Experimental Sensor-Bed System

This chapter explains the ballistocardiogram and details the sensor-bed setup, including the properties and functionality of the electromechanical films (EMFis) and load cells. The ability to acquire BCGs non-invasively with the sensor bed is an important step toward continuous health monitoring and improvement of quality of life. This chapter will also outline the modifications needed to convert the sensor bed to obtain mixed BCGs from two people that share the bed, including the resulting changes in acquired BCGs.

3.1. The Ballistocardiogram

During each heartbeat, the forces from the injection of blood into the vascular system result in a small alteration to the body's center of mass. To maintain the same center of mass, the body recoils slightly to counter-balance this force. This resulting recoil, measured as a force signal versus time, is known as the ballistocardiogram (BCG). The BCG forces propagate from the heart to the body in all directions, where the measured forces depend on the position and orientation of the associated sensor(s). The largest force component is the head-to-foot BCG, which represents the forces along the longitudinal axis. The transverse BCG is a measure of the anteroposterior or dorso-ventral forces, and the right-to-left BCG corresponds to the BCG forces in the lateral axis. For a person lying supine on a sensor-laden bed, the primary BCG component is along the dorso-ventral axis, although it is inevitable that an acquired BCG will be mixed, containing components that have a vector contribution along the other two axes.

Time-aligned ECG and BCG data are illustrated in Figure 3. Mechanical wave propagation in tissue is slow in comparison with electrical (ionic) activity gathered with electrodes, so a BCG IJK complex occurs at a later time than its counterpart ECG QRS complex. Information related to pulse rate and HRV can be determined from the resulting HBIs. Existing methods for peak detection were reviewed in *Chapter 2*.

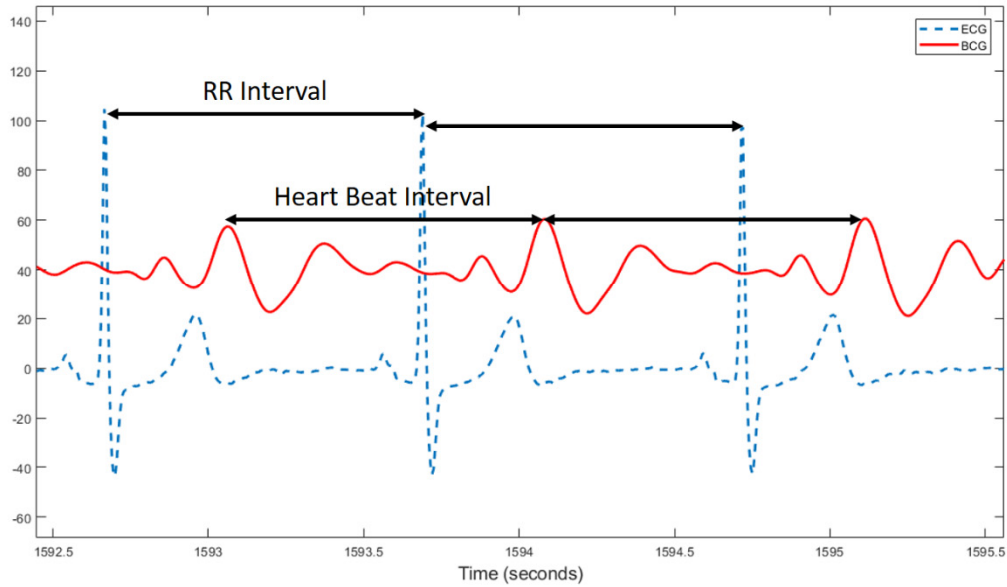


Figure 3. Time-aligned ECG and BCG waveforms.

3.1.1. BCG Waveform Description

Ballistocardiographic forces propagate in all directions, and the features of a BCG can vary greatly depending on the location and sleeping position of the person in addition to the location and orientation of the sensor. Figure 4 presents BCG waveforms that differ depending on sleeping position. Each BCG waveform also contains spring-mass components from the mattress which are also transduced by the force sensor. The added artifact from the mattress and additional subject movement make time-domain BCG analyses more difficult, even when these artifacts are attenuated with a preprocessing filter.

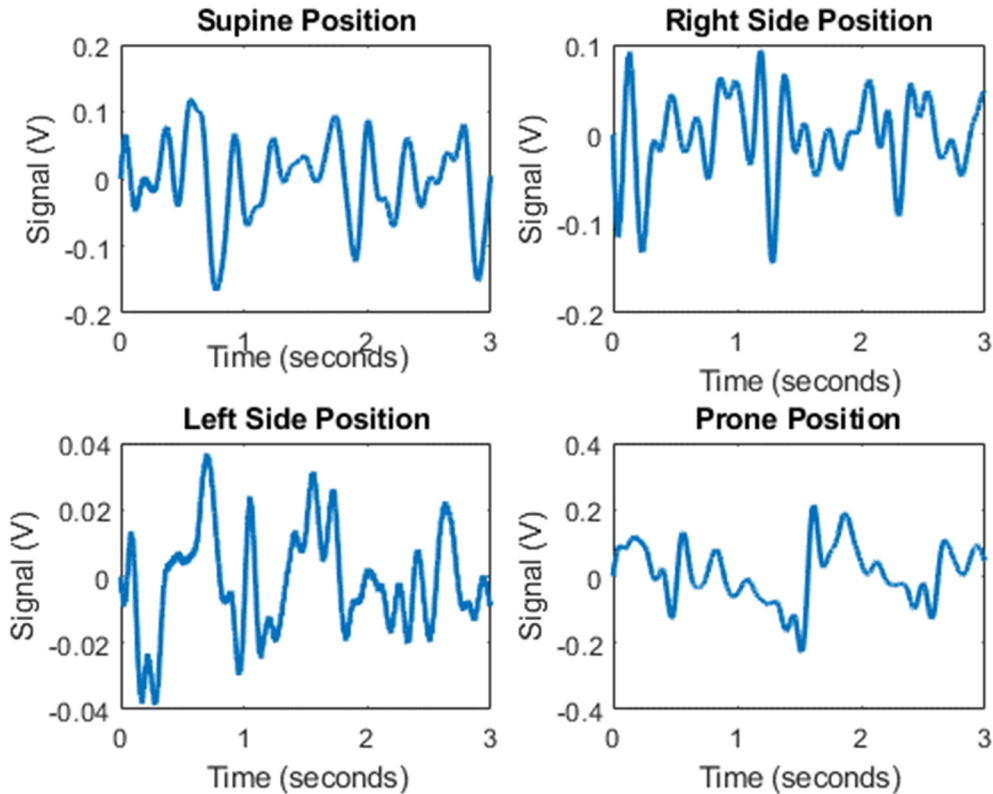


Figure 4. BCG waveforms acquired with EMFis for common sleeping positions: (top left) supine, (top right) right side, (bottom left) left side, and (bottom right) prone.

3.2. Bed Setup and BCG Acquisition

3.2.1. Bed and Film Setup

The sensor bed instrumentation was developed by a team at Kansas State University (KSU) – see Carlson *et al.* [2]. The bed utilizes four 300 mm x 580 mm electromechanical films (EMFit; L series) placed within pockets sown into the underside of a mattress cover in a 4 x 1 array, as illustrated in Figure 5. The films sit between the bed platform and the *underside* of the mattress to prevent damage to the EMFis that can occur when a subject lies directly on top of the films. The full sensor-bed configuration also contains four load cells (TE Connectivity Measurement Specialties; FX1901-0001-0200-L), where one load cell is placed under each of the four bed posts. The load cells have the advantage that they are not as sensitive to mattress vibrations when compared to the films, but load cell signals can be more easily corrupted by external ground vibrations caused by people walking, doors opening/closing, or objects dropped on the ground.

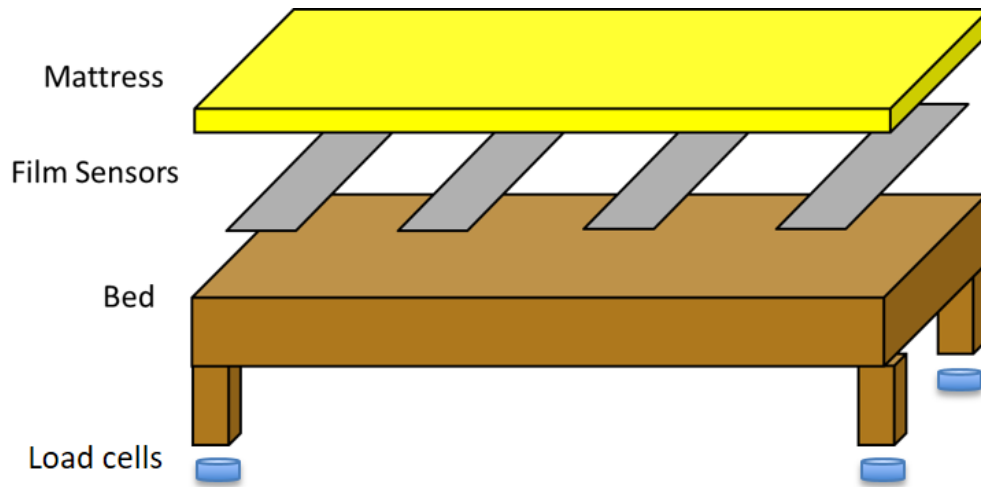


Figure 5. EMFi and load cell configuration on the sensor bed.

An EMFi is made up of three layers: two thin homogenous outer layers and one thicker inner layer, all of which are stretched during the manufacturing process in both the longitudinal and transverse directions. The inner layer is full of gas voids separated by what are described as ‘leaf-like polypropylene (PP) layers,’ where the voids are similar to electric dipoles and are easily compressed in thickness given applied pressure. An EMFi will experience a change in electrical charge distribution with any applied physical force, consistent with a change in film thickness [25]. In the case of this bed system, the physical forces will be the ballistic forces created by the heart. The output voltage of an EMFi sensor due to applied force can be calculated as

$$\Delta V = \left(\frac{1}{C}\right) \cdot S \cdot \Delta F, \quad (3.1)$$

where C is the capacitance, S is the sensitivity coefficient of the sensor, and ΔF is the impact force. With cellular polymers, large values of S can be achieved. A typical S value for a 70 μm thick EMFi is 170.

While a single, well-placed EMFi may be sufficient to acquire BCG data from an adult laying on the bed, the use of four films provides coverage for all areas of the bed, driven by the knowledge that a child, for example, does not always sleep in a supine position and may move to any area of the bed during the night. Additionally, the extra sensors provide redundancy plus

additional observations that can be used in the signal separation process, which becomes evident in *Chapter 5*.

In the bed system, each load cell measures force (typically weight) by producing a differential voltage when a static or dynamic force is applied, due to the Wien Bridge contained within the load cell. Load cells have proven valuable not only because they offer alternative means to record BCG data, but they do so in a different way, which can bypass disadvantages posed by the films. For example, unlike a film, a load cell can measure static (unchanging) force, which can be useful to determine a person's presence on the bed as well as their center of position. Figure 6 depicts a photo of the EMFis on a bed as well as a close-up of a load cell.

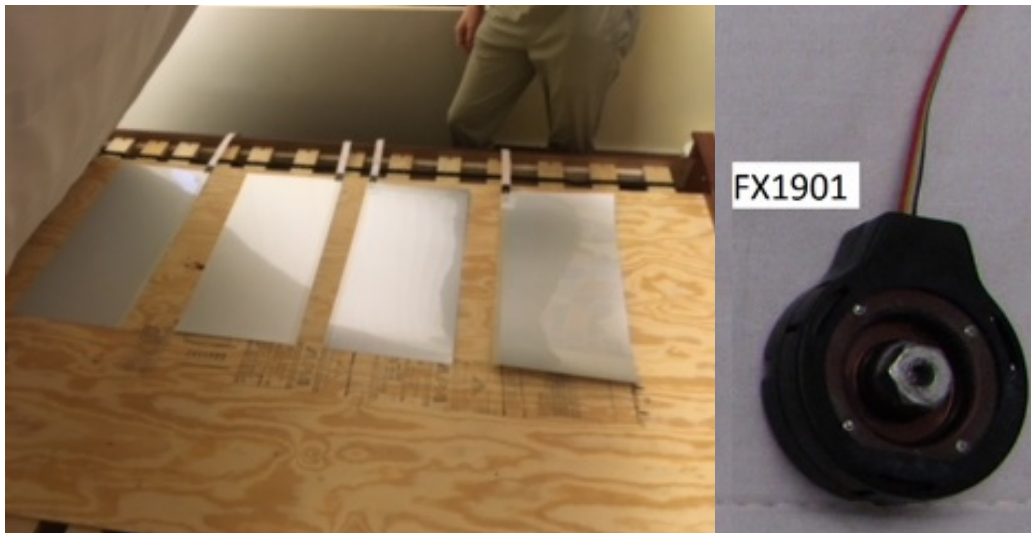


Figure 6. Two types of sensors employed by the sensor bed: (left) EMFis arranged in a 4 x 1 array underneath the mattress, and (right) load cell to be placed under each bedpost.

3.2.1. BCG Acquisition

Continuous BCG data are acquired from each individual EMFi and load cell. With each heartbeat, the displacement forces consistent with the recoil of the body are acquired as BCG recordings. Since BCG forces propagate in all directions through the body and the bed, the sensor measurement direction and location become important factors when a person lies down on the bed. For purposes of this section, the transverse (dorso-ventral) BCG was primarily collected from an EMFi located under the chest of a subject (Film 2 – see Figure 10 in *Chapter 3*).

Any resulting change in an EMFi charge distribution is amplified by a charge amplifier. For each film sensor, an inverting amplifier and a bandpass filter with a passband of 0.3 to 24 Hz are used in cascade to increase signal strength and improve signal quality, in part by removing 60 Hz power line noise [2]. For each load cell signal, a passband of 0.05 to 40 Hz is utilized. The resulting signals are digitized using a sampling frequency (f_s) of 1000 Hz and recorded with the help of a National Instruments (NI) LabVIEW virtual instrument (VI). Data are collected from the four EMFis using an NI 9220 module connected to an NI 9184 Ethernet cDAQ chassis. Acquired data are processed in MATLAB: they are digitally filtered to remove the DC baseline and 60 Hz power line noise. The respiration baseline is more prominent in the film signals when compared to the load cell data, so a high pass filter with a 0.5 Hz cutoff frequency is applied to EMFi BCGs to attenuate the respiration components. As previously mentioned in *Chapter 2*, respiration is an important health parameter, and the respiration of the subject can be obtained from the film data due to the prominence of the respiration component within the spectrum, so the attenuation of respiration components from load cell BCGs is purely due to the desire for a higher quality signal and spectrum. Frequency-domain spectra of unfiltered BCGs obtained with EMFis and load cells are depicted in Figure 7.

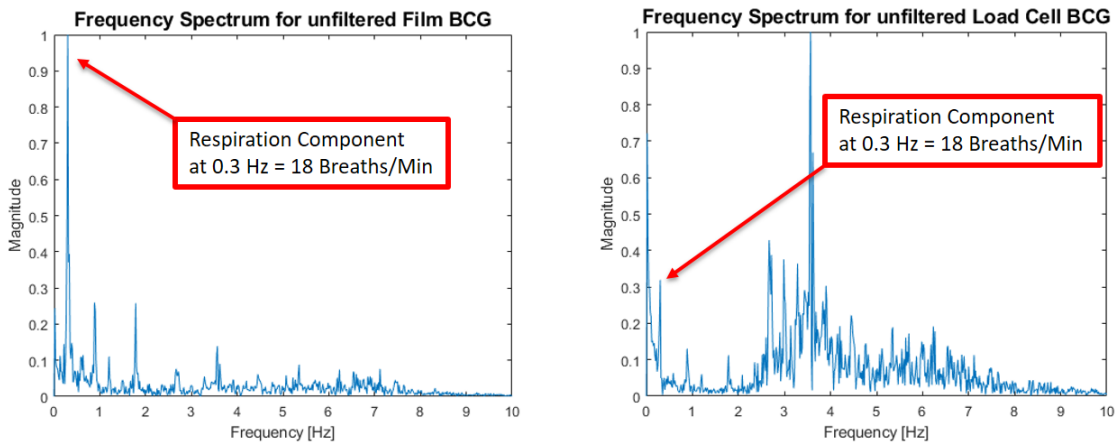


Figure 7. Frequency spectra of unfiltered BCGs recorded using an EMFi (left) and a load cell (right). The respiration component is prominent in the spectrum from the EMFi.

3.2.3. Signal Processing

Due to the high sensitivity of both the films and the load cells, substantive additive noise is present in these data. This noise can be a result of motion artifact from subject movement or

even vibrations from footsteps on the floor, so proper filtering is important. In summary, each channel in the system utilizes three types of filters: an analog lowpass filter during data collection, a digital highpass filter during data acquisition, and another digital lowpass filter prior to BCG analysis. These filters are put in place to minimize the effects of additive noise, allowing for more accurate signal separation and pulse rate estimation.

The mixed BCG data collected from the sensor bed with LabVIEW are zero-phase filtered in MATLAB using the `filtfilt()` function to improve signal quality. A finite impulse response (FIR) highpass filter with a cutoff frequency of 0.5 Hz attenuates the DC and respiration components in the load cell data, as respiration usually lies within the 0.2 Hz to 0.33 Hz range, corresponding to 12 to 20 breaths per minute. For EMFi data, the respiration rate is determined prior to filtering, and then a zero-phase FIR lowpass filter with a cutoff frequency of 25 Hz is applied to both the EMFi and load cell data to remove 60 Hz noise. Filtered and unfiltered EMFi BCG segments can be seen in Figure 8.

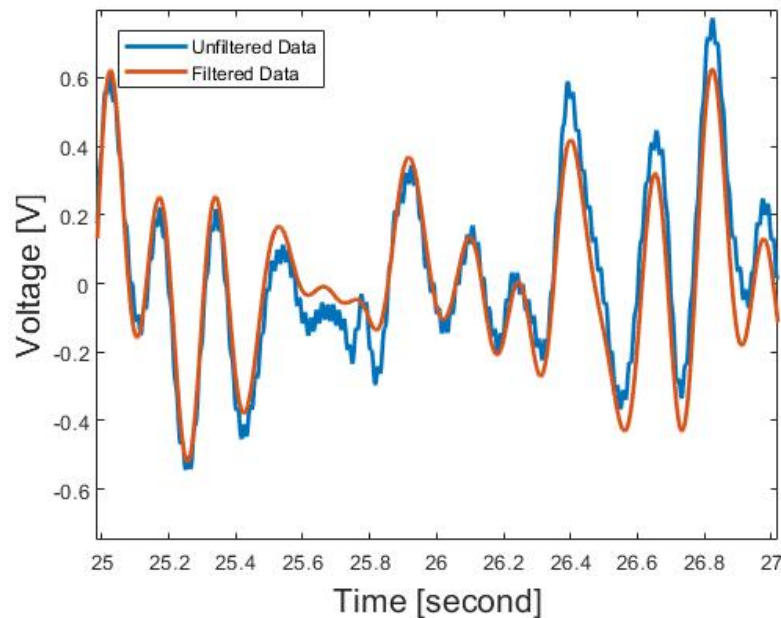


Figure 8. Unfiltered and filtered EMFi BCG segments.

3.3. Two-Body Problem

The aforementioned sensor-bed setup has proven useful for the collection of BCG data from a single individual sleeping in various positions [16]. This is a major step toward unobtrusive

at-home sleep monitoring and sleep quality assessment, but many people share a bed with another individual. With two subjects on the bed, the sensors will record mixed BCGs composed of the ballistic forces from both subjects, as illustrated in Figure 9. Separation of this mixed signal into two separate BCGs can be a challenge because the source signals have similar fundamental frequencies and their frequency spectra overlap. A mixed BCG displays few distinct waveform characteristics or properties, if any, that are usually distinguishable with a single-person BCG. Therefore, typical heart beat interval algorithms will not work, since they are tailored to look for features present in single-person BCGs. To make unobtrusive at-home sleep monitoring accessible to the everyday home, the problem of mixed BCGs must be addressed.

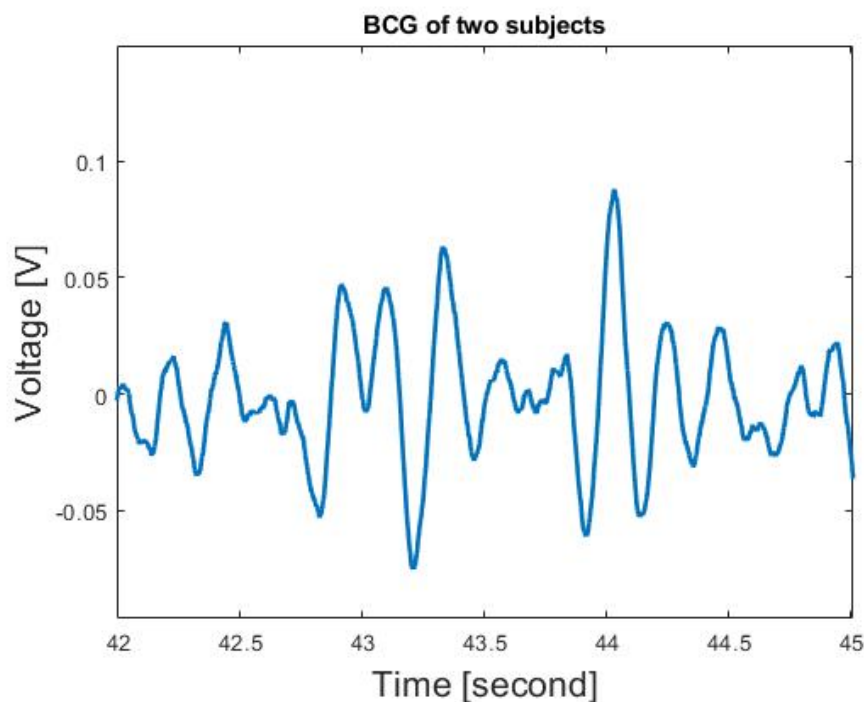


Figure 9. A three-second segment of a mixed BCG, recorded using an EMFi, for two subjects lying in supine positions on a shared bed. From the plot, there are no distinct features which could be used to visually identify the pulse rate of each individual.

Minor modifications were made to the sensor-laden, single-person bed to be suitable for two people: the mattress and frame were switched to a full-size bed, and slight changes were made to the EMFi sensor layout, but the same NI data acquisition setup was employed. Both EMFis and load cells were employed: the EMFis were positioned in two different configurations (see Figure

10 below) while the four load cells were once again positioned underneath the four bedposts as in the single-bed setup.

Mixed BCG data were collected in two-minute segments from pairs of healthy adults of various combinations of ages and genders. All subjects laid in a supine position, and data were collected at the Kansas State University Lafene Health Center. As it is difficult, arguably impossible, to obtain subjects' individual and mixed BCGs simultaneously, the results of the BSS separation process were not verified by comparing the separated BCGs to the corresponding single-person BCGs, but rather by comparing the pulse rates estimated from the separated source signals to independently acquired pulse rates. To do this, the team utilized a CardioCap 5 patient monitor to collect one subject's ECG and the other subject's PPG during each two-minute segment. A combination of the Pan-Tompkins algorithm and visual observations verified these ground truth values. Due to the desire to obtain 1 bpm resolution in these BCG frequency spectra, BCG recordings were acquired in one-minute segments. Since the Pan-Tompkins algorithm provides an estimated heart rate for each ECG R-R interval, the average heart rate for each one-minute segment was compared against BCG estimates.

3.3.1. Film and Load Cell Setup

To determine the optimal signal separation method, one must understand how the mixed signals are recorded. More specifically, to successfully perform source separation, the number of recording devices must be greater than or equal to the number of sources. For the two-body scenario, a total of at least two films and/or load cells must provide data to pursue source separation. This sensor-bed configuration contains more than the required number of sensors, so these extra film and load-cell signals contribute to the robustness of the system, plus the extra information can offer more successful signal separation. The load cell locations were fixed under the bedposts, but different film-placement configurations were considered, and ultimately two configurations were employed – see Figure 10:

Configuration 1: All four EMFi sensors under one subject

Configuration 2: Two EMFi sensors under each subject

Configuration 1 emphasizes data from a single subject, while *configuration 2* gives equal emphasis to both subjects.

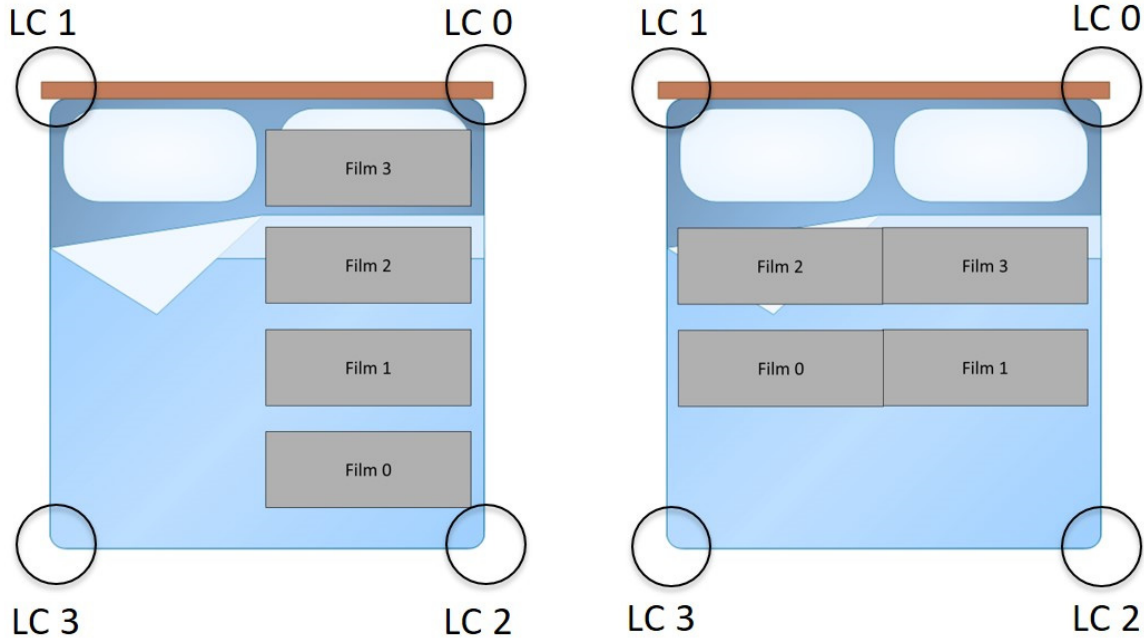


Figure 10. EMFi placement configurations: (left) all four EMFi films placed directly below one subject, and (right) two films placed directly under each subject.

Two types of mattresses were used for data collection: a soft spring mattress and a hard-spring mattress. The type of mattress affects the propagation of the ballistic forces: a harder spring mattress provides greater BCG damping, meaning a BCG will not propagate as freely through the mattress when compared to a soft spring mattress. It is well known that spring-mass behavior of a mattress can alter BCG data [3]. The goal of using a hard spring mattress was to minimize or eliminate this undesired artifact, but if the mattress is too hard, the ballistic forces may not propagate as easily through the mattress, affecting the BCG signal-to-noise ratio.

3.3.2. Pulse Rate Determination

The method employed here to determine the pulse rates of two subjects from a mixed BCG involves two processes.

1. A technique that utilizes a form of ‘source separation’ to split the mixed BCG into its individual components.
2. A pulse estimation technique that employs a frequency-domain, peak-ranking algorithm to determine the pulse rate of each subject from the corresponding separated signal.

This overall process is illustrated in Figure 11. Mixed BCGs are collected from EMFis and load cells using a LabVIEW VI, which also receives ECG and PPG data from the CardioCap 5 sensors attached to each person on the bed. These data are processed in LabVIEW, stored, and transferred to MATLAB, where a separation algorithm estimates the source signals, $s_1(t), \dots, s_N(t)$. A frequency-based pulse estimation algorithm is applied to each separated signal. Comparing the estimated pulse rate of each subject to their pulse rate as determined from ECG/PPG data allows for assessment of the effectiveness of these algorithms. Such an assessment will also allow the team to observe changes in algorithm performance as a function of changes in the monitoring environment (e.g., changes in film configurations and mattress type).

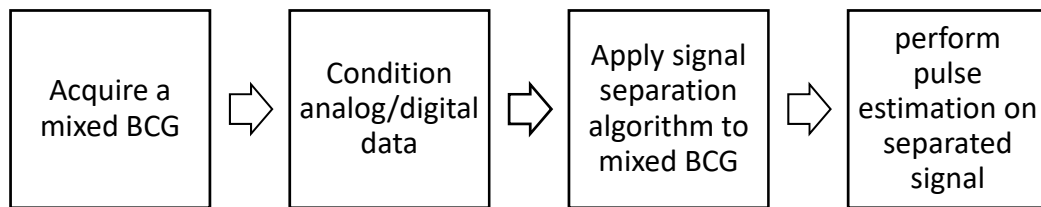


Figure 11. Flow diagram detailing the process of estimating pulse rate from mixed BCGs.

Chapter 4 - Pulse Rate Estimation Method

This chapter addresses a method to estimate a subject's pulse rate from their BCG by applying a frequency-domain, peak-scoring algorithm which seeks to identify the fundamental harmonic (i.e., the frequency corresponding to pulse rate) based on certain criteria applied to the various spectral peaks. Unlike time-domain methods that seek to identify cardiac cycles based on particular waveform features, this frequency-domain method possesses the advantage that the actual shape of the BCG waveform is secondary to the frequency of reoccurrence. This is an important trait when considering the separation technique in *Chapter 5*, since separated BCGs often lose some of the characteristics which are important to traditional time-domain, pulse-rate estimation algorithms. The peak-scoring algorithm was developed and tested using single-person BCGs, and its performance is addressed later in *Chapter 6*.

4.1. Peak Scoring Algorithm

A lack of prominent J peaks exists within certain BCGs as a result of waveform variations that can be attributed to different sleeping positions, measurement techniques, and mattress characteristics. It is therefore difficult to utilize time-domain peak-detection methods similar to those employed to determine heart rate from ECG R peaks. While a variety of methods have been proposed for BCG pulse rate estimation [11, 22, 48, 54-55], the majority of these methods do involve looking at time-domain peaks in an attempt to determine heart beat intervals and heart rate variability. BCGs exhibit a variety of shapes, but they share a common property: each cycle of a given BCG has roughly the same fundamental shape, even if that shape does not exhibit a classic IJK waveform feature. This repetitive BCG nature can be exploited to determine pulse rate. The method employed here looks to the frequency domain to identify the fundamental harmonic frequency, f_1 , directly (i.e., the harmonic that corresponds to cycle recurrence and thus pulse rate) based on the positioning of this component relative to the other harmonics in the frequency spectrum. The BCG frequency spectrum is not unexplored territory. Others have sought to estimate pulse rate using the cepstrum method [23] or by finding the 3rd harmonic frequency, f_3 , of a BCG measured using fiber optic sensors affixed to a headrest [24].

4.1.1. BCG Frequency Domain Spectra

Time-domain variations in BCGs lead to variations in their counterpart frequency spectra, as seen in Figure 12. In each of these different spectra, the harmonic associated with the pulse rate is not always the most prominent harmonic: the most prominent harmonic can be the 2nd, 3rd or even 4th harmonic. Due to this uncertainty, an algorithm cannot simply seek the highest spectral magnitude and then identify pulse rate as corresponding to the associated frequency. For a time-domain signal that is pseudo-periodic in character, it is well known that the base period of the waveform results in a fundamental spectral harmonic at a frequency, f_1 , and that distinctive higher harmonics will exist at frequencies that are integer multiples of f_1 . With this information, the method described below seeks to accurately estimate f_1 by identifying those higher frequency harmonics. If those harmonics exist and have prominent peaks, the method assumes that f_1 and its corresponding pulse rate have been identified.

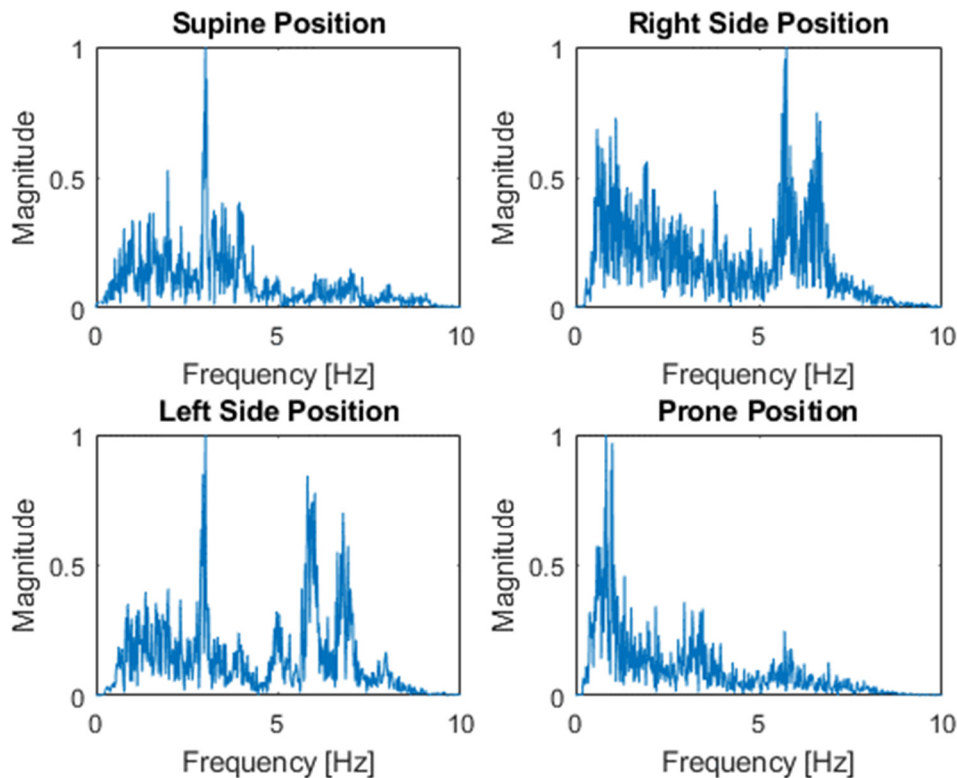


Figure 12. BCG frequency spectra of 60-second segments acquired for various sleeping positions: (top left) supine, (top right) right side, (bottom left) left side, and (bottom right) prone. Sleeping position affects the strongest harmonic in the frequency spectrum.

4.1.2. Algorithm Ranking Technique

Resting BCG pulse rate frequencies for an average adult typically lie within the range of 0.5 to 2 Hz (30 to 120 beats per minute) [47]. The algorithm presented here seeks to identify a pulse rate within this expected range by assessing the character of the various frequency-domain harmonics within a spectrum. A peak-scoring algorithm for use with PPGs, toward the determination of pulse rate and blood oxygen saturation, was developed by Kaestle in the mid 1990s [35]. That technique, which serves as the inspiration for the method utilized here, scores peaks in the frequency spectrum based on certain criteria. The highest scoring harmonic is determined to be the fundamental harmonic whose frequency corresponds to the estimated pulse rate. The peak-scoring algorithm used here with BCGs employs a similar technique to identify and score peaks. While time-domain PPGs and BCGs are different in structure, the peak-scoring principles of the algorithm can be applied in light of the general existence of the fundamental and secondary harmonics within a BCG spectrum.

This technique applies a Fast Fourier Transform (FFT) to a filtered BCG to observe its magnitude spectrum, focusing on the frequency range between 0 Hz and 10 Hz. While cardiac activity extends beyond 10 Hz in the frequency domain, resting pulse rates do not typically exceed 2 Hz. A sliding window with a duration of 1 minute is incorporated to obtain BCG segments, where successive windows are generated in one-second increments (i.e., the window overlap is 59 seconds). The one-minute interval arises from the desire for a 1 bpm resolution in the spectrum: each spectral bin represents $1/(60 \text{ sec}) \approx 0.0167 \text{ Hz}$, or 1 beat per minute. Zero-padding was not employed to artificially improve the spectral resolution since the peak-scoring method depends on an accurate spectral shape. There is a clear tradeoff between the desire for a better frequency resolution and the desire for a smaller time segment. Since the pulse rate estimated from the frequency spectrum represents an average pulse rate over the time window, the value in this parameter diminishes as the window is widened. This widening can reduce, e.g., the effectiveness of a secondary parameter such as HRV.

The algorithm first identifies the highest 10 peaks within the range of 0.5 to 2 Hz, where a peak within 0.01 Hz of another selected peak cannot be identified. The highest 10 peaks within the range of 2 to 4 Hz are then identified; these serve primarily as the associated 2nd and 3rd harmonics. Finally, the highest 5 peaks within the range of 4 to 8 Hz are identified; these serve primarily as

the 4th to 6th harmonics. This results in a total of 25 peaks; a representative set is plotted in Figure 13. While a prominent peak can sometimes be claimed to exist at a frequency, f_l (i.e., the fundamental frequency), experience dictates that this is often not the case. In a BCG, the time-domain waveform shape that corresponds to the fundamental period is somewhat nondescript; most of the oscillations that drive features of interest such as the I, J, and K peaks occur at higher frequencies more consistent with secondary harmonics. Additionally, the frequency-domain components associated with the mattress response are also contained in these spectra. As a result, a number of peaks may need to be identified to correctly specify f_l and the associated higher harmonics. It is possible to over-identify the peaks, meaning that as the number of identified peaks increases, there are now more peaks which can potentially be identified as f_l . Therefore, due to the nature of the algorithm, increasing the number of potential peaks in any of the three frequency ranges can work to either increase or decrease accuracy. Kaestle *et al.* used 10 total peaks for their algorithm [35], but that number is sufficient because a PPG not corrupted by motion artifact typically offers a couple of clear fundamental peaks (e.g., for respiration rate and pulse rate) accompanied by four or five clear secondary harmonics. For BCGs, empirical trials have indicated that 10 peaks within the 0 to 2 Hz range is a good number, as this allows the identification of weaker peaks otherwise buried by dominant peaks that may be a result of artifacts.

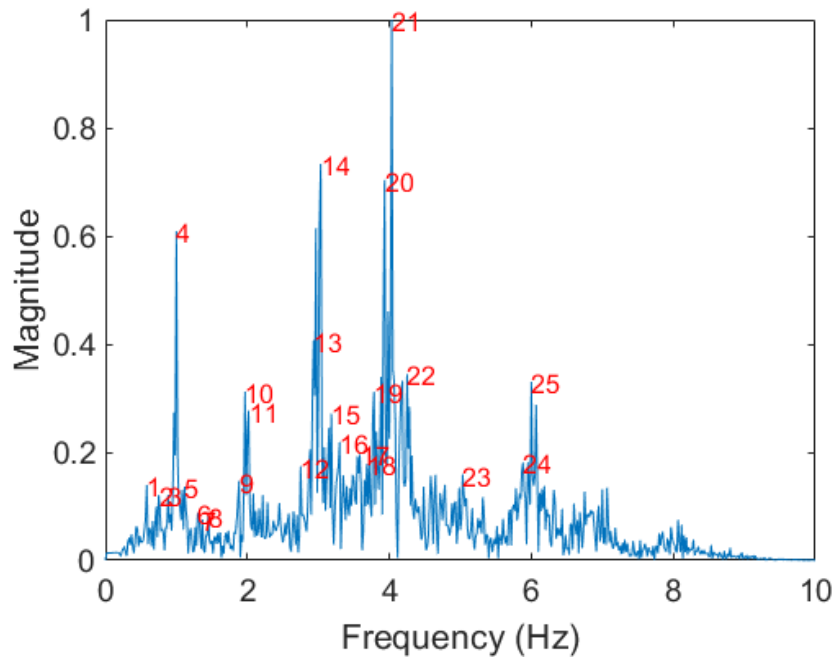


Figure 13. Spectrum of a 60-second film-based BCG segment with the identified peaks numbered. The prominent peak (#21) is the 4th harmonic.

The pseudocode used to find and score peaks is as follows.

```

while (Read data)
{
  Sliding Window of X seconds in length
  for (i = 1 to length of data incrementing in X*Fs)
  {
    Compute single-side spectrum, normalize magnitude
      Find 10 highest peaks within 0.5 Hz to 2 Hz; sort in ascending
      order by frequency
      Find 10 highest peaks within 2 Hz to 4 Hz; sort in ascending
      order by frequency
      Find 5 highest peaks within 4 Hz to 8 Hz; sort in ascending
      order by frequency

    Locate highest peak within the entire spectrum (frequency and
    index)
    While(Read data)
    {
      Run Data through Harmonic Ranking function -> Obtain
      scores from first run
      Run Data through 2nd Harmonic Ranking function -> update
      scores, tabulate results
    }
    Plot data
  }
}

```

The pseudocode used for harmonic ranking function is as follows.

```
While (Read data)
{
    peak1 = peak being scored/assessed
    peak2 = peak being compared with
    for (j = 1 to length of data)
    {
        Reset counted to false
        for (i = 1 to length of data)
        {
            Determine ratio  $P(i,j) = i^{\text{th}} \text{ peak1} / j^{\text{th}} \text{ peak2}$ 
            If (ith peak2 == highest peak)
            {
                If (P(i,j) is within 5% of either 2, 3, or 4)
                {
                    Score based on scoring criteria
                }
            }
            If (P(i,j) is within 1% of either 2, 3 or 4)
            {
                Set counted to true to avoid recounting
                Score based on scoring criteria
            }
            If (P(i,j) is within 5% of 5)
            {
                Set counted to true to avoid recounting
                Score based on scoring criteria
            }
        }
    }
    For (k = 1 to length of data)
    {
        If (counted is false)
        {
            If (P(k,j) is within 5% of either 2, 3 or 4)
            {
                Set counted to true to avoid recounting
                Score based on scoring criteria
            }
        }
        If (counted is false)
        {
            If (P(k,j) is within 10% of 5)
            {
                Set counted to true to avoid recounting
                Score based on scoring criteria
            }
        }
        If counted was true for 2, 3, 4 & 5
        {
            Score based on scoring criteria
        }
    }
}
}
```

The pseudocode for the second harmonic ranking step is as follows.

```
While (read data)
{
  For (i = 1 to length of data)
  {
    If (magnitude of ith peak is the highest peak)
    {
      Score based on scoring criteria
    } else if (magnitude of ith peak is > 70% of highest peak) {
      Score based on scoring criteria
    } else if (magnitude of ith peak is within 50% to 70% of
highest peak) {
      Score based on scoring criteria
    }
    If (pulse rate of ith peak is within 50 to 90)
    {
      Score based on scoring criteria
    }
    If (pulse rate of ith peak is outside of 50 to 90)
    {
      Score based on scoring criteria
    }
  }
  Find highest two peaks
  if(highest peak is more than 70% greater than 2nd highest peak)
  {
    Score based on scoring criteria
  }
}
```

Points are assigned to each peak as they fulfil the following criteria.

For each integer multiple within 1% of another harmonic (for the 2nd, 3rd & 4th harmonics)

- +20 if peak2 is > 70% of highest magnitude peak
- +15 if peak2 is within 30% to 70% of highest magnitude peak
- +10 otherwise

For each integer multiple within 5% of another harmonic (for the 2nd, 3rd & 4th harmonics)

- +15 if peak2 is > 70% of highest magnitude peak
- +10 if peak2 is within 30% to 70% of highest magnitude peak
- +5 otherwise

For each integer multiple within 5% of another harmonic (for the 5th & 6th harmonics)

- +12 if peak2 is > 70% of highest magnitude peak
- +7 if peak2 is within 30% to 70% of highest magnitude peak
- +3 otherwise

For each integer multiple within 10% of another harmonic (for the 5th & 6th harmonics)

+10 if peak2 is > 70% of highest magnitude peak

+5 if peak2 is within 30% to 70% of highest magnitude peak

+1 otherwise

+20 points if integer multiple within 5% of highest magnitude peak

Additional +20 points if the peak1 is the highest peak

Additional +10 points if peak1 is the highest peak and is more than 70% higher than the next highest peak.

+15 points if peak1 magnitude is within 70% of the highest peak

+5 points if peak magnitude is within 50% of the highest peak

+20 points if peak's associated pulse rate lies within the probable pulse rate 40 to 90 beats per minute.

+15 points if there exists a multiple of 2, 3, 4 & 5 amongst all peak2

Each integer value can only be counted once

Points are deducted for the following criterion

-100 points if outside of the optimal range 0.5 Hz to 1.5 Hz, this will render the harmonic out of consideration as f_i .

The point allocations for the above criteria are loosely based off of the point system utilized by Kaestle *et al.* in [35]. While Kaestle *et al.* allocated fixed points for the fulfilment of each criterion, the decision to score based on the respective magnitude of the peak was added due to the greater number of peaks and incidentally higher harmonics involved.

Scores are tallied for each peak, and the peak with the highest score is determined to be the fundamental peak with a frequency, f_i . In the event that two peaks receive the same score, the peak with the largest magnitude is determined to be the fundamental peak. Once the fundamental peak is identified, pulse rate in beats per minute (bpm) is an easy conversion.

As an example, consider the one-minute BCG segment whose spectrum is depicted in Figure 13. Peaks 1 to 10 are the highest-magnitude peaks in the range of 0.5 to 2 Hz, and peaks 11 to 20 are the highest-magnitude peaks in the range of 2 to 4 Hz. Finally, peaks 21 to 25 are the highest-magnitude peaks in the range of 4 to 8 Hz. Each peak is scored based on the criteria

mentioned above, and the results are tabulated in Table 1. From the scores in Table 1, it is evident that the primary peaks of interest are the first ten peaks. Peak 4 scored the highest with a score of 113, so this peak is considered to be associated with a pulse rate of 60 bpm.

Table 1. Example peak scoring and ranking for the spectrum in Figure 13.

Peak	Frequency (Hz)	Magnitude (Relative %)	Pulse Rate (BPM)	Score
1	0.5833	13.921	35	12
2	0.75	12.04	45	18
3	0.8833	12.13	53	47
4	1	60.898	60	113
5	1.1167	13.621	67	45
6	1.3	8.7085	78	75
7	1.3667	7.5523	82	75
8	1.45	8.1605	87	55
9	1.8833	14.687	113	20
10	1.9667	31.192	118	50
11	2.0167	27.676	121	-45
12	2.75	17.401	165	-100

Figure 14 contains a linear flow diagram for the peak-scoring process, which includes a frequency-domain analysis to extract the signal’s primary components and obtain pulse rate estimates for all eight BCGs – four from EMFi and four from load cells. Filtering is included to produce a measurement as close to ground truth as possible. The first filtering step (step 7 in Figure 14) involves an assessment of all four measurements from each type of sensor (four EMFi measurements and four load cell measurements) to produce a single pulse rate value. Finally, a sliding median window is added to help account for instantaneous variations in pulse rate that are not sensible when compared to recent pulse rates.

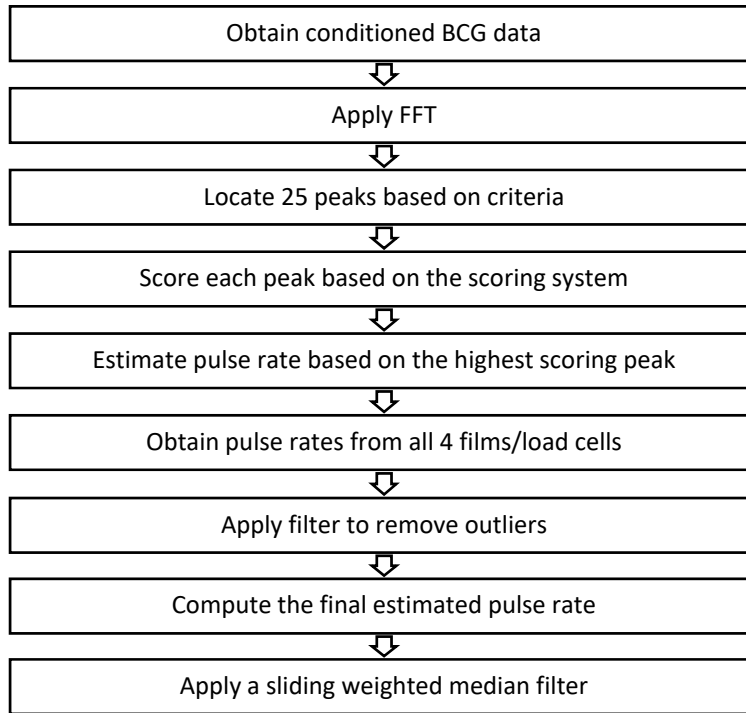


Figure 14. Overall process associated with the peak-scoring algorithm.

Variability exists in BCGs acquired from different parts of the body, meaning each film records different signals, which also depend upon the subject’s sleeping position. Due to this variability, and to fully utilize the four-film bed system, an additional algorithm was implemented to identify the most probable pulse rate from all four films. The code looks at the estimated pulse rate from each of the four sensors, and if these rates are the same or within an acceptable range of 2 bpm relative to one another, then the result is obvious. If a clear outlier is present, the outlier is ignored, and the other three values are assessed.

The effects of this algorithm are evident in the results in Table 2, which displays pulse rate results for the four BCG segments depicted in Figure 13. In Table 2, pulse rates from film 0 and film 1 are locally inconsistent with the pulse rates determined from the other three EMFis. This can result from various factors, including motion artifact, mattress spring components, or a weak SNR for a given film or load cell (e.g., as film 0 is positioned at the feet – see Figure 10 (left)). With the addition of the selection algorithm, the film 0 results for three out of the four time segments are identified as outliers and thus ignored. The same situation applies to film 1 for time segment four. The estimates from the remaining three EMFis are utilized in each case, and the

overall results are more consistent with the pulse rates as measured using an ECG for the same time intervals.

Table 2. Estimated pulse rates for four 1-minute BCG segments from four EMFis for a subject lying in a supine position.

ECG (BPM)	Film 0 (BPM)	Film 1 (BPM)	Film 2 (BPM)	Film 3 (BPM)	After Selection Algorithm (BPM)	% Error
57.870	63	59	59	59	59	1.95 %
61.747	66	60	61	61	61	1.21 %
60.277	56	61	60	60	60	0.46 %
59.827	60	63	60	60	60	0.29 %

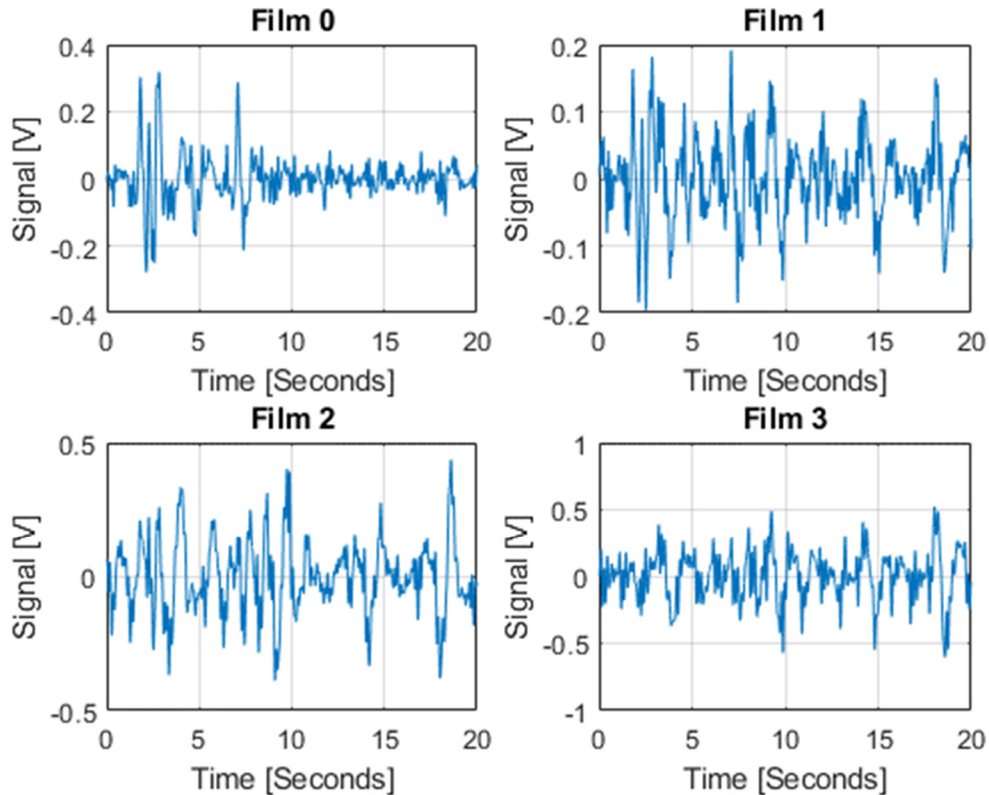


Figure 15. BCG segments collected from each of the four films during the same time interval as in Table 2. Minor subject movement appears just before the 5-second mark, but only the BCGs from films 0 & 1 were affected in a major way.

A final median sliding window filter was added, as noted in Figure 14, to track pulse rate changes over time and to ensure that reported pulse rates are locally consistent in comparison with prior values. The sliding window moves in one-second increments, and the processing algorithm obtains the estimated pulse rate for each consecutive one-minute segment. The pulse rate from the previous time window is gathered and used for comparison, and after five values are obtained in this manner, sequential pulse rate estimations are determined based on the current pulse rate compared with the average from previous five rates. This was done to minimize the effects of local outliers on reported values: outliers due to, e.g., motion corruption or poor BCG signal quality due to sleeping position/location.

The frequency-domain approach has its own limitations, the most impactful being the need to obtain one minute of data prior to providing a result, which means the reported pulse rate will be delayed by at least one minute. While this delay is unacceptable for a clinic setting, the focus of this application is sleep monitoring, which ideally spans the entire night and equates to hours of data, where post-processing is a primary goal. A one-minute delay is therefore relatively insignificant. The advantages of a frequency-domain approach, however, are numerous. Perhaps the greatest advantage is that the peak-scoring algorithm can be applied to the spectra of BCGs that have a variety of shapes, even if those BCGs do not display traditional BCG features. This benefit becomes critical, as will be evident later in *Chapters 5 and 6*, which address mixed BCGs acquired from two people that share a sensor bed. When mixed BCGs are separated into their estimated component signals, these separated signals may not be exact representations of the ideal BCGs, but certain waveform characteristics will remain, including their time-domain periodicity and their frequency-domain harmonics. By capitalizing on these frequency-domain features, a fundamental frequency, f_1 , and the corresponding pulse rate can still be identified for a person even if their separated time-domain waveform is an imperfect BCG representation.

Chapter 5 - Two Body Problem

This chapter sets out to address the scenario where two subjects lie on the sensor bed, meaning that the recorded BCGs from each sensor are a mixture of these individuals' BCGs. A time-domain BCG mixture does not resemble a single-person BCG, so it is difficult to apply traditional pulse rate estimation methods utilized for single-person BCGs. Likewise, the frequency spectrum of a mixed BCG bears little resemblance to the spectrum of a single-person BCG. To extract the pulse rate for one or both individuals, a method must first be applied to separate a mixed BCG into its component sources. Here, a mixed signal is first separated in the time domain before the previously mentioned frequency-domain, peak-scoring algorithm is applied to determine pulse rate for each person.

5.1. Two-person BCG Frequency Domain Spectrum

Chapter 3 introduced the notion that BCG waveforms change shape in the time domain when two people lie on a sensor bed, so it should come as no surprise that BCG spectra also change character as a result of the additional person. Figure 16 depicts the frequency spectrum of a one-minute segment of a mixed BCG acquired from two individuals lying on a shared sensor bed. The fundamental, 2nd, and 3rd harmonics for the original BCGs are nearly impossible to differentiate. Since each person's heartbeat forces differ, BCG spectral components from one person may be more dominant than the components from the other person. This implies a possibly lower SNR for one subject and a higher SNR for the other. This effect is more visible when EMFi *configuration 1* is used (see Figure 10), due to all of the sensors being placed directly under one subject.

The practical result of mixing two BCGs is that the frequency domain spectrum is no longer suitable for, e.g., a peak-scoring algorithm to determine pulse rate. In a mixed spectrum, two fundamental harmonics are present, along with their associated secondary harmonics. This renders the peak-scoring algorithm ineffective. Therefore, the mixed BCG must first be separated into its individual BCGs before the pulse rates of the respective individuals can be determined. The following section addresses this process.

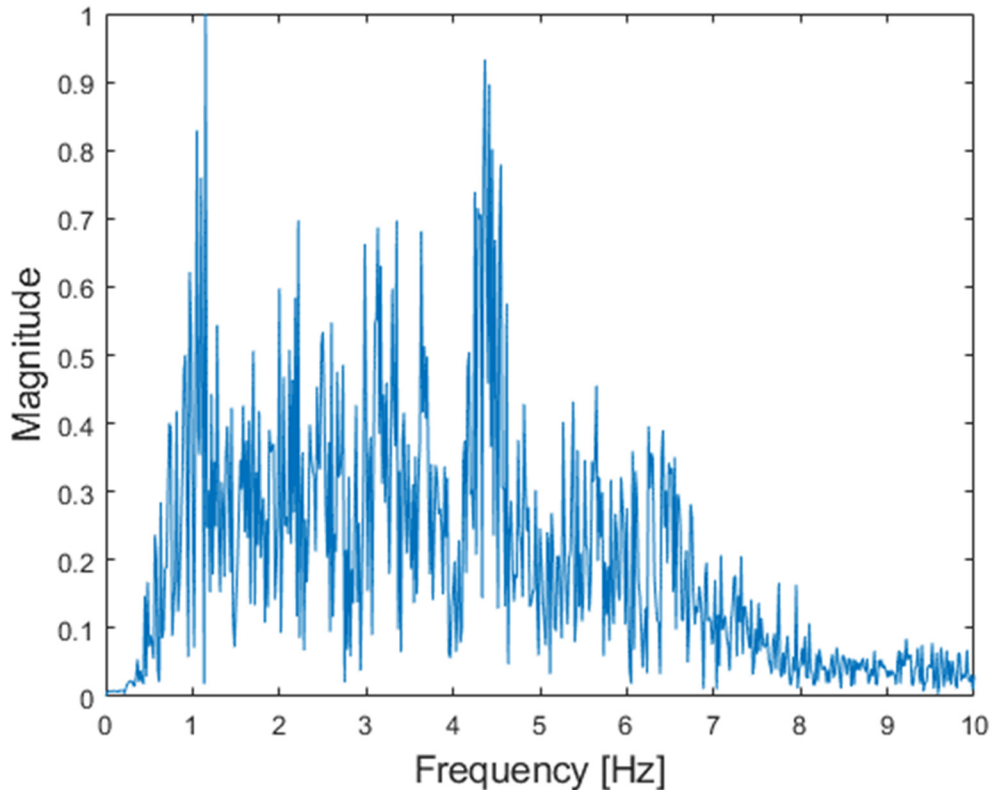


Figure 16. Frequency spectrum of a mixed BCG, where each of the two individuals is lying on the bed in a supine position

5.2. Signal Separation Applied to Mixed BCGs

The challenges associated with the separation of mixed BCGs were stated in *Chapter 1*:

- Cardiac activity present within BCGs exists at low frequencies.
- Frequency components and spectral behavior can be common in different people.
- Forces propagate through a mattress in every direction.
- BCGs from two individuals cannot be assumed to be mutually independent due to the shared mattress.

While many BSS variants exist, the majority of these techniques assume and require mutual independence between the signal sources. This mutual independence is a property that cannot be assumed, so other forms of source separation are needed where dependence can be assumed or independence is not required.

5.2.1. Independent Component Analysis

Independent component analysis (ICA), as discussed in *Chapter 2*, is one of the most commonly used methods to separate unknown source signals based off of only the observed mixed signals [9, 39]. Recall that at each time, t , the simple noiseless mixing model is defined as

$$\mathbf{x}(t) = \mathbf{A}\mathbf{s}(t) , \quad (5.1)$$

where $\mathbf{x}(t)$ is the observed signal, \mathbf{A} is the mixing matrix, and $\mathbf{s}(t)$ is the source signal vector. The main separation criterion is the independence amongst the elements in the source signal, $\mathbf{s}(t)$. To separate the mixed signals, mixing matrix \mathbf{A} must be invertible and identified, leading to the separation matrix, $\mathbf{Q} = \mathbf{A}^\#$, where $\#$ denotes a Moore-Penrose pseudo-inverse.

Given how ICA decomposes signals, two major parameters are unavailable after separation:

1. the exact amplitudes of the signals, and
2. knowledge of which signal belongs to which subject.

While the missing amplitude information is not an issue, since each signal can be normalized if required, the latter poses an immediate problem. In certain applications, assistance from human eyes is required to manually assign separated sources to observations (for example, with mixed images). For this sensor-bed study, ground-truth pulse rates are available to assess the separation process. This allows for the association of separated signals, $\mathbf{s}_1(t)$ and $\mathbf{s}_2(t)$, with each respective subject. In practice, however, no prior knowledge is available regarding a subject's pulse rate. Subject identification is a topic that will require further attention.

5.2.2. Multidimensional Independent Component Analysis

Multidimensional independent component analysis (MICA) is an extension of ICA, possessing the same goal to separate N underlying sources, \mathbf{s} , given M observations. However, unlike standard ICA processes, MICA allows some sources to have common statistics. Using a similar model, MICA groups each component into k -tuples, each of size k . Each of the \mathbf{s}_i components within each subspace is assumed to be dependent on the other components, but each grouping of k -tuples is independent from the other k -tuple groupings. In the case where $k = 1$, the model simplifies to the standard ICA model, where the k -tuples can theoretically each contain a

different number of s_i components. For simplicity, it is generally assumed that each grouping of k -tuples contains an equal number of components.

The ICA model in Equation 5.1 can be rewritten as an additive model as opposed to a multiplicative one:

$$\mathbf{x} = \sum_{p=1}^N \mathbf{x}_p, \quad (5.2)$$

where \mathbf{x}_p is defined as:

$$\mathbf{x}_p \stackrel{\text{def}}{=} \mathbf{a}_p \mathbf{s}_p \quad \text{for } 1 \leq p \leq N. \quad (5.3)$$

The model presented in Equation 5.2 is more closely related to traditional principal component analysis (PCA). This new ICA model is matrix-free and contains a different parameterization than its multiplicative counterpart in Equation 5.1. In Equation 5.2, the smallest subspace containing the p^{th} component is referred to as the component subspace for the p^{th} component. The orthogonal projector onto this subspace is denoted by $\mathbf{\Pi}_p$ and can be expressed as

$$\mathbf{\Pi}_p \stackrel{\text{def}}{=} \frac{\mathbf{a}_p \mathbf{a}_p^T}{\mathbf{a}_p^T \mathbf{a}_p}, \quad 1 \leq p \leq N. \quad (5.4)$$

Matrix $\tilde{\mathbf{\Pi}}_p$ is the projector onto the p^{th} component space and is orthogonal to all of the other components:

$$\mathbf{x}_p = \tilde{\mathbf{\Pi}}_p \mathbf{x} \quad (5.5)$$

and

$$\tilde{\mathbf{\Pi}}_p \stackrel{\text{def}}{=} \left(\sum_{q=1}^N \mathbf{\Pi}_q \right)^{\#} \quad (5.6)$$

where $\#$ denotes a Moore-Penrose pseudo-inverse. In the MICA decomposition model, the mixing matrix is no longer of interest. Instead, attention shifts towards

$$\mathcal{P} = \{\mathbf{\Pi}_1, \dots, \mathbf{\Pi}_N\},$$

which is the set of orthogonal projection matrices onto each component space. The standard ICA model in Equation 5.1 has now been transformed into a geometric ‘component model’ without any indeterminacies. This perspective leads to the more general MICA model:

$$\mathbf{\Pi}_p = \mathbf{A}_p (\mathbf{A}_p^T \mathbf{A}_p)^{-1} \mathbf{A}_p^T, \quad 1 \leq p \leq c. \quad (5.7)$$

Using MICA decomposition, the mixed BCG data are provided to the JADE algorithm [38] to determine $\hat{\mathbf{A}}$: an estimate of the mixing matrix, \mathbf{A} . Multiplying \mathbf{A}^{-1} by the observations, \mathbf{x} , yields an estimated set of four source signals, $\hat{\mathbf{S}}$. While the next part typically requires human observation to differentiate which component belongs to which subject, visual inspection of the values in $\hat{\mathbf{S}}$ (using a pulse estimation technique) gives a close approximation regarding which values belong to which signal source, by observing different pulse rates from each observation. This indicates which component is extracted by the algorithm and with which column in \mathbf{A} each component is associated, allowing the estimation of the orthogonal projector of each subject using Equation 5.7. Figure 17 portrays mixed BCGs gathered from four EMFis when two individuals lie on the bed in a supine position. Utilizing the MICA decomposition algorithm, the mixing matrix, $\hat{\mathbf{A}}$, is estimated using the JADE algorithm, which was discussed in *Chapter 2*. While JADE cannot be used to efficiently separate the signals due to the lack of mutual independence, the estimated mixing matrix is sufficient to determine which signals the algorithm has extracted and placed within each vector of $\hat{\mathbf{A}}$.

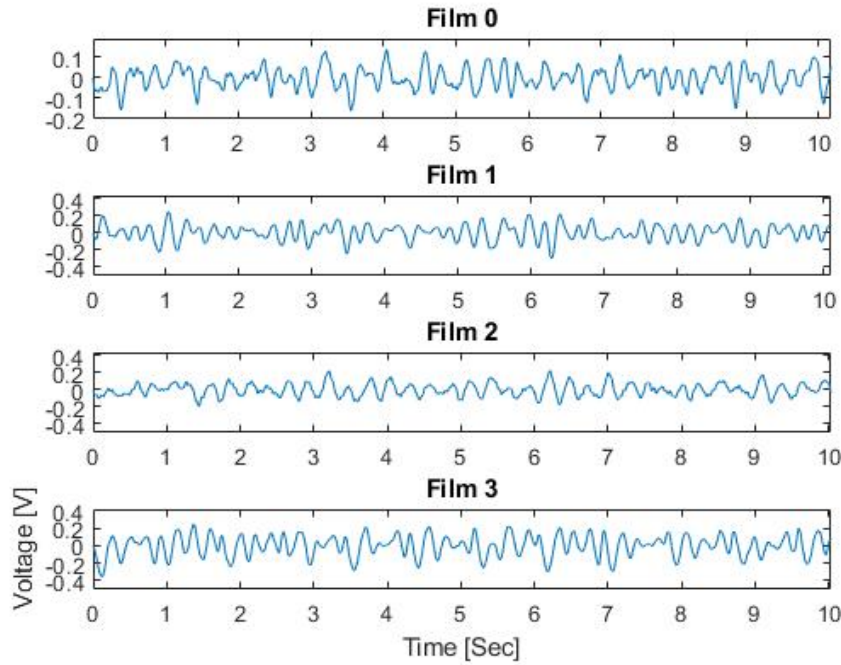


Figure 17. Mixed BCGs gathered from four EMFIs when two people lie on the bed.

For the signals presented in Figure 17, the JADE algorithm results in the following estimate of the 4×4 mixing matrix, $\hat{\mathbf{A}}$:

$$\hat{\mathbf{A}} = [\hat{a}_1 \quad \hat{a}_2 \quad \hat{a}_3 \quad \hat{a}_4] \approx \begin{bmatrix} 0.0350 & 0.0177 & 0.0241 & -0.0008 \\ -0.0509 & -0.0469 & 0.0391 & -0.0175 \\ 0.0201 & 0.0190 & 0.0140 & -0.0520 \\ 0.0720 & -0.0636 & -0.0299 & -0.0107 \end{bmatrix}.$$

Finding the inverse, $\hat{\mathbf{A}}^{-1}$, and applying it to the BCG mixtures, $\hat{\mathbf{S}} = \hat{\mathbf{A}}^{-1}\mathbf{X}$, yields the estimated signals, $\hat{\mathbf{S}}$, as depicted in Figure 18. Observations of the signals in $\hat{\mathbf{S}}$ are required to determine which components are extracted by the algorithm and in which column the algorithm has placed each component. This process is typically performed manually by visual inspection since the original intention was to separate mixed ECGs which possess distinct R-peaks. BCGs are difficult to analyze, yet it is desirable to automate this process, so the peak-scoring algorithm is employed (a) to observe the pulse rate of each observation in the signal, $\hat{\mathbf{S}}$, and (b) to determine which components are extracted by the algorithm based on the estimation results from $\hat{\mathbf{S}}$.

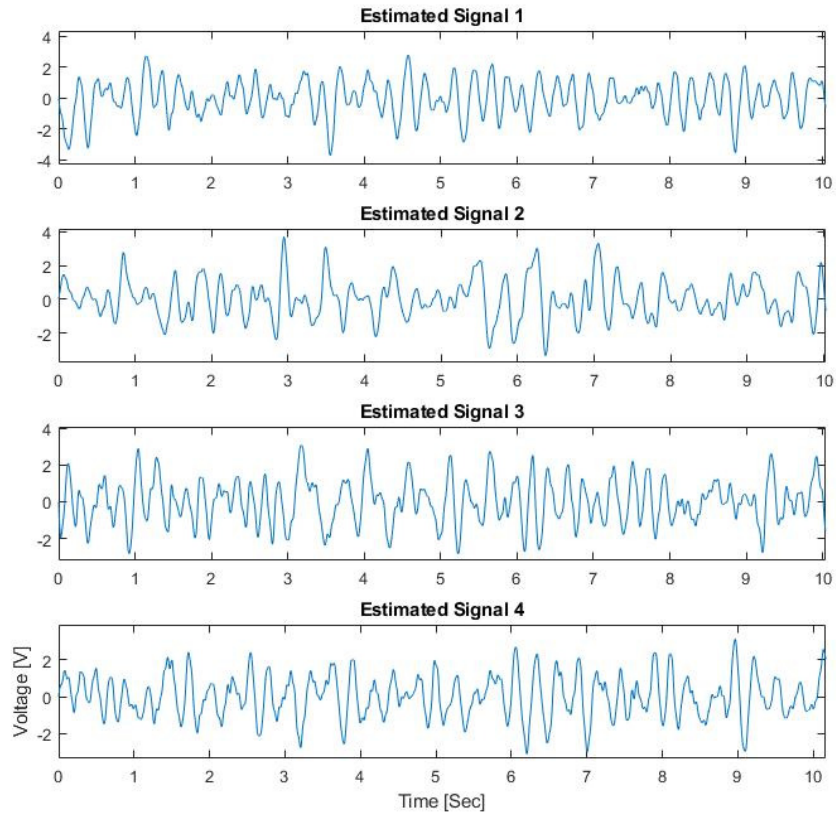


Figure 18. Estimated signals, $\hat{\mathbf{S}}$, using the estimated separation matrix, $\hat{\mathbf{A}}^{-1}$, produced by running the JADE algorithm.

Each signal component is projected onto its respective subspace given the results obtained from utilizing the peak-scoring algorithm on $\hat{\mathbf{S}}$. The signal with the highest estimated pulse rate is assigned to subject A, while the signal with the lowest pulse rate is assigned to subject B. The remaining estimates are assigned depending on their ‘closeness’ to the pulse rate for either subject A or subject B:

```

If |maximum - pulse rate| >= |pulse rate - minimum|
    Assign to Subject A
Otherwise
    Assign to Subject B
End

```

Applying the peak-scoring algorithm from *Chapter 4* to the signals in Figure 18 yields the results in Table 3. These results reveal that the algorithm has extracted two source signals for

subject A (with estimated pulse rates of approximately 61 bpm) and two source signals for subject B (with estimated pulse rates of approximately 53 bpm). These data were modeled by MICA decomposition into two bi-dimensional components (for subject A and subject B). Since subject A's signal appears in the first two columns, subject A's subspace is estimated as the orthogonal projection matrix Π_A onto $[\hat{a}_1 \ \hat{a}_2]$, and the orthogonal projection Π_B for subject B's subspace is $[\hat{a}_3 \ \hat{a}_4]$.

Table 3. Estimated pulse rates after applying the peak-scoring algorithm to the estimated signals, \hat{S} .

	Est. Signal 1	Est. Signal 2	Est. Signal 3	Est. Signal 4
Pulse Rate [BPM]	61.3043	61.3043	53.4783	53.9130

Using Equation 5.7, the orthogonal projections for subjects A and B are defined as

$$\Pi_A \approx \begin{bmatrix} 0.2027 & -0.3640 & 0.1454 & 0.0896 \\ -0.3640 & 0.6957 & -0.2787 & 0.0396 \\ 0.1454 & -0.2787 & 0.1116 & -0.0197 \\ 0.0896 & 0.0396 & -0.0197 & 0.9899 \end{bmatrix}$$

$$\Pi_B \approx \begin{bmatrix} 0.2026 & 0.2839 & -0.0255 & -0.2833 \\ 0.2839 & 0.4841 & 0.2381 & -0.3354 \\ -0.0255 & 0.2381 & 0.8728 & 0.2317 \\ -0.2833 & -0.3354 & 0.2317 & 0.4405 \end{bmatrix}$$

Applying Equation 5.6 to the above yields

$$\tilde{\Pi}_A \approx \begin{bmatrix} 0.4578 & -0.2598 & -0.0681 & -0.0608 \\ -0.6948 & 0.5552 & -0.1921 & 0.0768 \\ 0.2750 & -0.2234 & 0.0781 & -0.0343 \\ 0.8050 & 0.3057 & -0.3012 & 0.9090 \end{bmatrix}$$

$$\tilde{\Pi}_B \approx \begin{bmatrix} 0.5422 & 0.2598 & -0.0681 & -0.0608 \\ 0.6948 & 0.4448 & 0.1921 & -0.0768 \\ -0.2750 & 0.2234 & 0.9219 & 0.0343 \\ -0.8050 & -0.3057 & 0.3012 & 0.0910 \end{bmatrix}$$

Equation 5.5 allows the reconstruction of subject A's and subject B's bi-dimensional components. The separated BCGs for subject A recorded with the four EMFis are depicted in Figure 19. Unfortunately, since it is difficult to obtain mixed BCGs and single-person BCGs simultaneously, the separated signals cannot be compared to the corresponding single-person BCGs to verify their shapes. For this reason, pulse rates for the separated signals were estimated and then compared to pulse rates obtained with simultaneous ECGs and PPGs. The spectrum for separated signal 1 in Figure 19 is depicted in Figure 20. Corresponding time- and frequency-domain plots for subject B are contained in Figure 19 and Figure 20. The frequency spectra in Figure 20 and Figure 22 display a clear fundamental peak when compared to typical two-person mixed BCG frequency spectra.

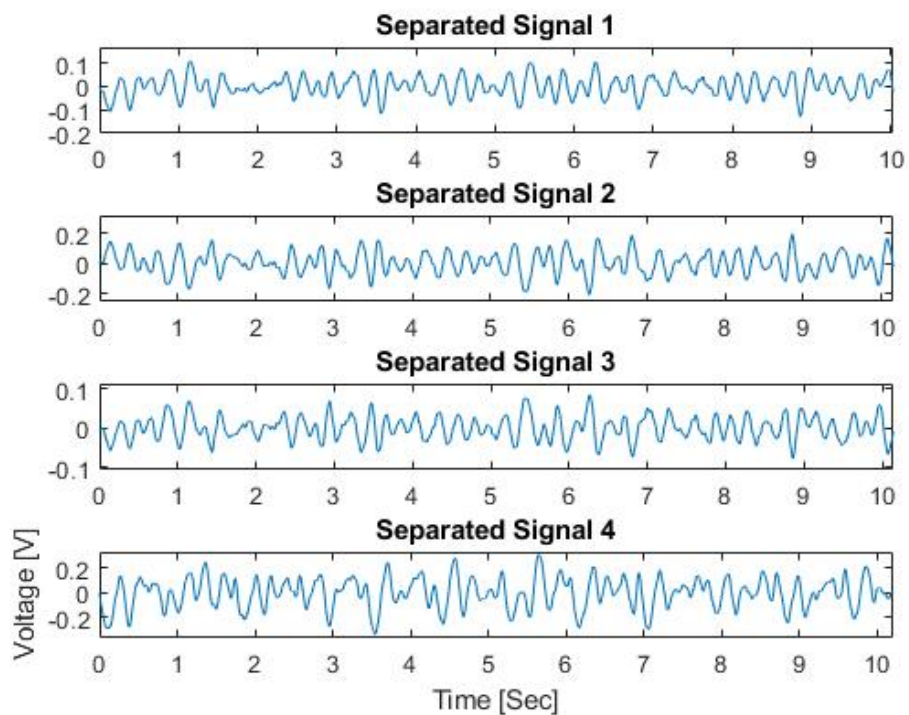


Figure 19. Separated signals acquired from all four films (subject A).

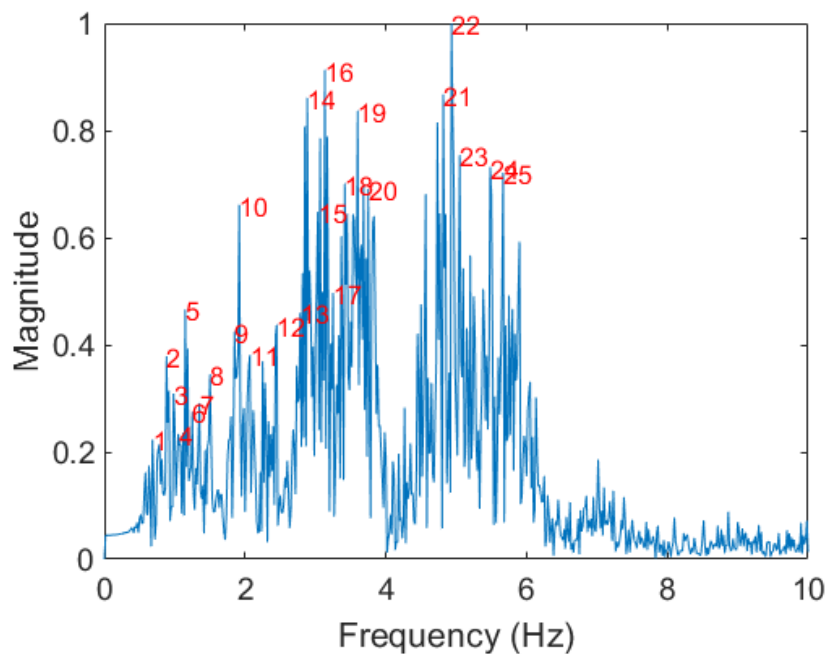


Figure 20. Frequency spectrum of a one-minute segment of separated signal 1 in Figure 19. A harmonic is visible at peak 5.

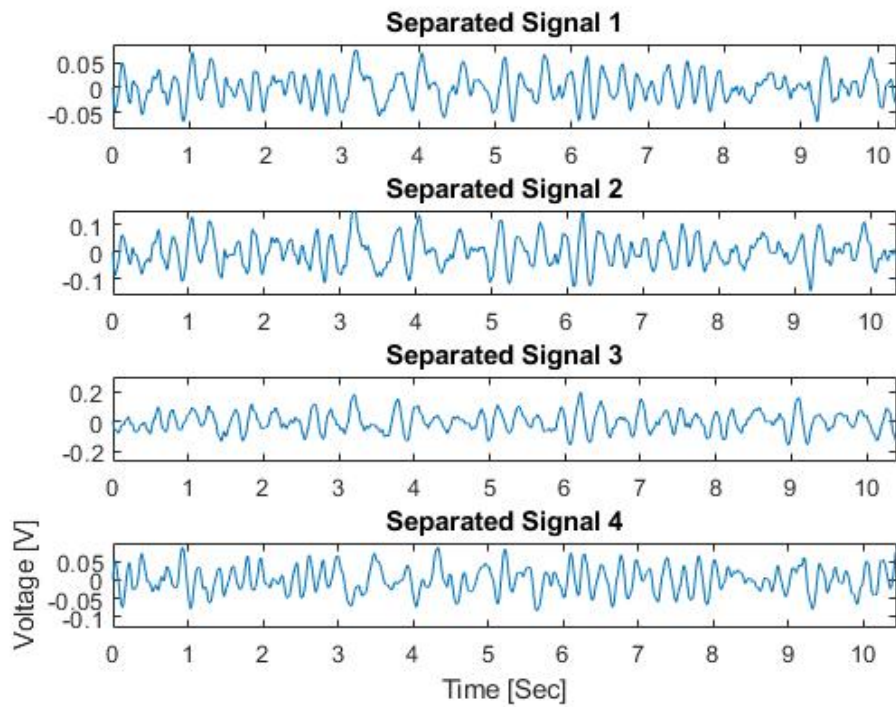


Figure 21. Separated signals acquired from all four films (subject B).

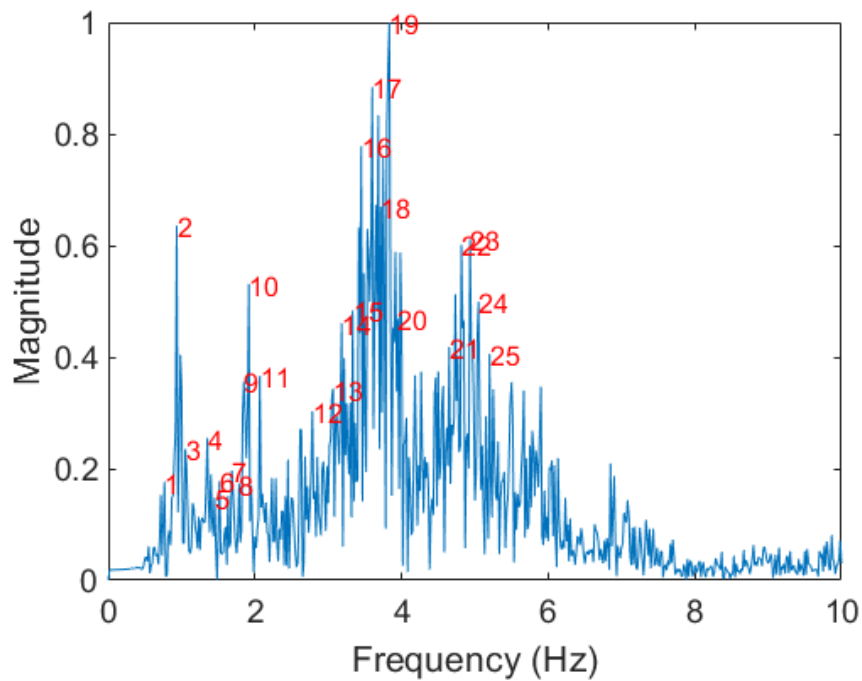


Figure 22. Frequency spectrum of a one-minute segment of separated signal 1 in Figure 21. A distinct harmonic is visible at peak 2.

Chapter 6 - Results and Performance

This chapter presents findings and results from both the peak-scoring algorithm and the overall combined algorithm for the estimation of pulse rates from mixed BCGs. The performance of the peak-scoring algorithm is evaluated for a single person laying on the sensor bed. Estimated pulse rates are gathered from both load cell BCGs and film BCGs, and these results are compared with ground truth pulse rates from simultaneous ECGs. This chapter also looks at how changes in the setup environment affect both algorithm performance and BCG quality. These environmental variables include sensor type, sleeping position, mattress type, and film configuration for a two-person scenario.

6.1. Acquired BCG Recordings

Five healthy adults volunteered for this short study: three males and two females, all members of the research team. The participant age was 30.3 ± 4.087 years (mean \pm stDev), ranging from 25 to 36 years. Subjects laid on the sensor bed for both single-person and two-person performance evaluations. For the single-person studies, only configuration 1 (all EMFis under one side of bed – see Figure 10) was used. The participant was asked to lay motionlessly on the sensor bed in each sleeping position (supine, right side, left side, and prone) for approximately two minutes. For the two-person studies, two participants laid on the sensor bed next to each other, and they were asked to lay still while breathing at a regular rate not monitored or defined. For simplicity, only the supine position was studied for the two-person scenario. Each participant was paired with every other participant, creating 10 different pairings.

6.2. Estimated Pulse Rates Using the Peak-Scoring Algorithm

Prior to addressing the separated signals, the performance of the peak-scoring algorithm must be evaluated using single-person BCGs collected with different sleeping postures and different mattress types. Simultaneous ECG data were collected from subjects to provide ‘ground truth’ pulse rates, where the Pan-Tompkins algorithm [10] determined beat-to-beat and aggregate pulse rates for each ECG data segment. Using the sliding window approach detailed in *Chapter 4*, the average pulse rate over the duration of each short study can be observed and compared to its

ECG counterpart. Both EMFi and load cell data were collected and evaluated, but the estimated results from either sensor type were not utilized together in any way for this study – the EMFi and load cell data were recorded and analyzed separately.

A Bland-Altman plot [46] (see Figure 23) compares the estimated BCG pulse rates over a set of time intervals to the ‘true’ ECG pulse rates acquired during those same time intervals. The Bland-Altman plot displays the difference between the respective measured and true pulse rates (dependent axis) as a function of the average of each set of measured and true pulse rates (independent axis). This type of plot is useful for analyzing the agreement between the outputs of two different procedures which are used to determine the same parameter. The Bland-Altman plot in Figure 23 is a representative plot that addresses pulse rates from all film and load-cell BCGs addressed in these studies. The individual study results, including errors in estimated versus ground-truth pulse rates, are addressed in the following sections.

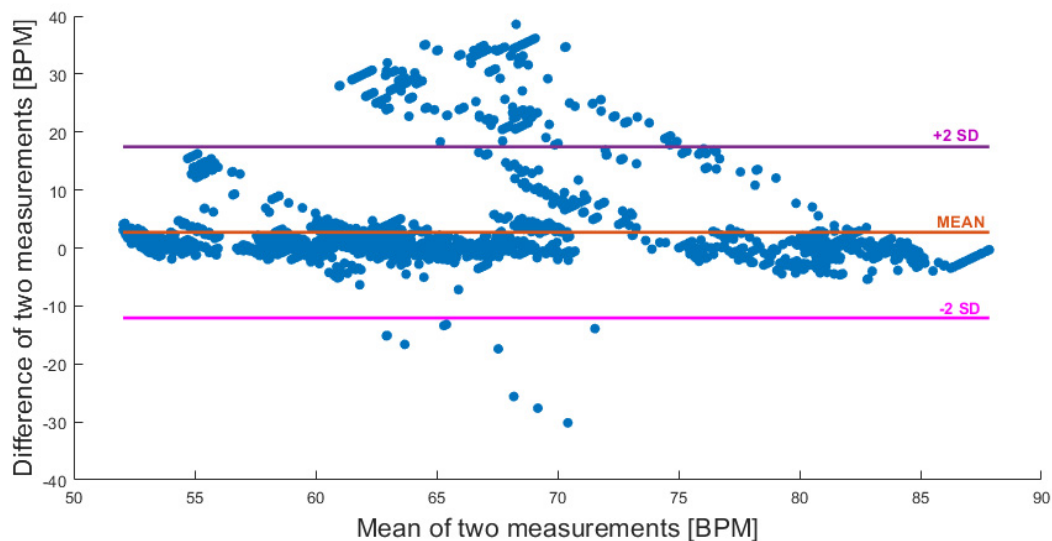


Figure 23. Bland-Altman plot comparing estimated pulse rates from BCGs to pulse rates from ECGs for both film and load cell sensors.

The error in the pulse rate estimates is determined by calculating the root mean squared (RMS) value of the differences between the pulse rates determined by the peak-scoring algorithm and the Pan-Tompkins approach. The RMS value is preferred because the simple addition of the positive and negative differences between the two measurements can result in an overall arithmetic

difference close to 0, yielding an artificial indicator for accuracy. The RMS value, x_{RMS} , of a set of n differences, x_n , is calculated using the expression

$$x_{RMS} = \sqrt{\frac{1}{n}(x_1^2 + x_2^2 + \dots + x_n^2)} \quad (6.1)$$

As mentioned in *Chapter 5*, a pulse rate as determined from the fundamental frequency in a spectrum represents the average pulse rate over the time interval represented by the spectrum. As such, a comparison of the average pulse rate for the time interval with the average ECG pulse rate over that same interval is appropriate. The difference between these two average pulse rates was recorded as an error, with the RMS value of the overall error determined using Equation 6.1.

6.2.1. Films Versus Load Cells

For this study, the performance of each EMFi and load cell was evaluated in terms of its ability to offer meaningful BCGs and commensurate pulse rates. Both types of sensors collect BCGs in unique ways and have proven beneficial. Data were acquired for 2 minutes from each of the 5 participants, resulting in a total of 160 two-minute-long segments, or 9,600 data points, for each of the eight bed sensors. Pulse rate estimates were determined from individual sensors and compared to the respective ‘true’ ECG and PPG pulse rates; the BCG pulse rates were not combined in any way. Representative single-person BCGs acquired with the eight EMFis and load cells are illustrated in Figure 24 for a four-second time interval.

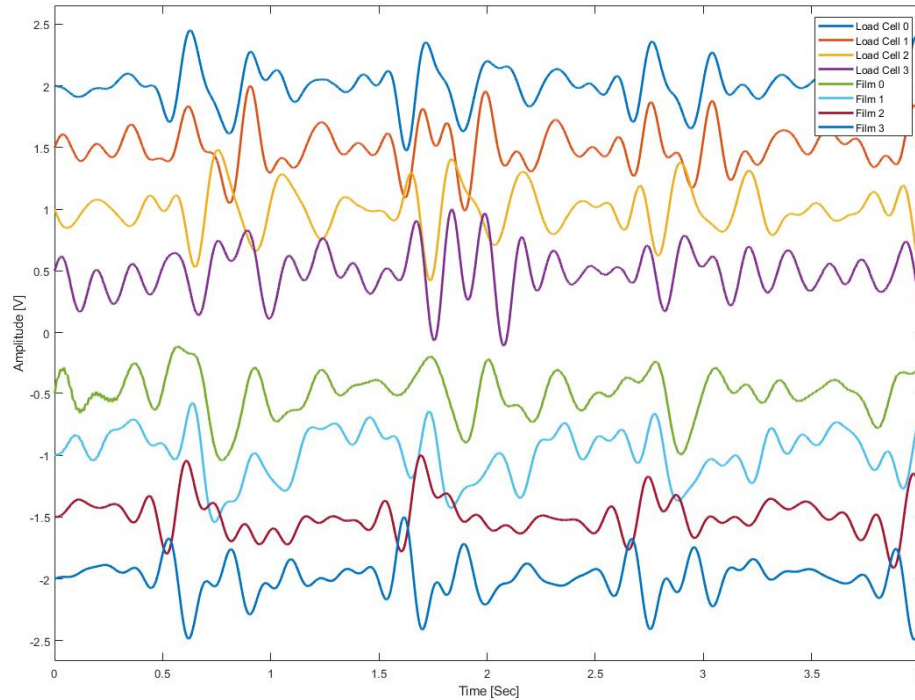


Figure 24. BCG recordings from EMFis and load cells for a single person on the bed. Slight differences in waveform patterns are apparent between the two sensor types.

In Figure 24, there are noticeable differences between the BCGs collected using films and the BCGs collected using load cells. While the general IJK complex is present in each of the BCGs, the waveform oscillations differ due to the medium and the sensor positioning relative to the chest of the subject.

The results for the peak-scoring algorithm (applied to the BCGs from the four films and the four load cells) were compared to the results obtained from the ECG pulse rates as calculated using the Pan-Tompkins algorithm. Since the peak-scoring algorithm estimates pulse rate using a one-minute BCG segment, the resulting value is an average over the whole time period. Since the ECG data allow pulse rate estimation based on each R-R interval, these intervals were averaged to determine an aggregate pulse rate for each minute of data. This means that if the pulse rate of the subject changes rapidly within the one-minute time span, the peak-scoring algorithm will not be able to adjust to the change.

The RMS values of the pulse rate errors for the film and load cell BCGs are displayed in Table 4. The films produced an average error of 12.38 bpm, while the load cells produced an average error of 1.69 bpm. These results indicate that the peak-scoring algorithm provides

reasonable pulse rate estimates for BCGs obtained utilizing load cells. However, assessment of the film data is a bit more complicated, as noted below.

Table 4. RMS errors for the pulse rates determined from film and load cell BCGs.

Sensor Type; Constraint	RMS Error (BPM)
Film; with respiration	12.38
Film; without respiration	3.44
Load cell	1.69

The film pulse rates display a significantly higher error than the load cell pulse rates, primarily due to the respiration harmonic being much more prominent in the film BCG frequency spectra. While the fundamental respiration harmonic is attenuated using a digital filter, the periodic respiration harmonics remain in the spectrum. The high magnitudes of the respiration harmonics present in film data often make these harmonics more prominent than even the fundamental pulse component. This effect creates extreme outliers in pulse rate estimation, which contribute to large errors. While this occurrence does not present issues under normal circumstances, in the event that the respiration harmonics and pulse rate harmonics share frequencies, this tricks the peak-scoring algorithm into labelling a respiration harmonic as the fundamental pulse component. These effects are illustrated in Figure 25 below, where the algorithm determines 1.0 Hz to be the fundamental pulse frequency due to the prominence of that peak and the number of harmonics that appear present at lower frequencies. In truth, the fundamental harmonic is actually 1.5 Hz, and the two features (respiration and pulse) share multiple common periodic harmonics. Removal of these rare occurrences yields an error of 3.44 with film-based BCGs (see Table 4). This error remains larger than its load cell counterpart, but it is now within an acceptable tolerance.

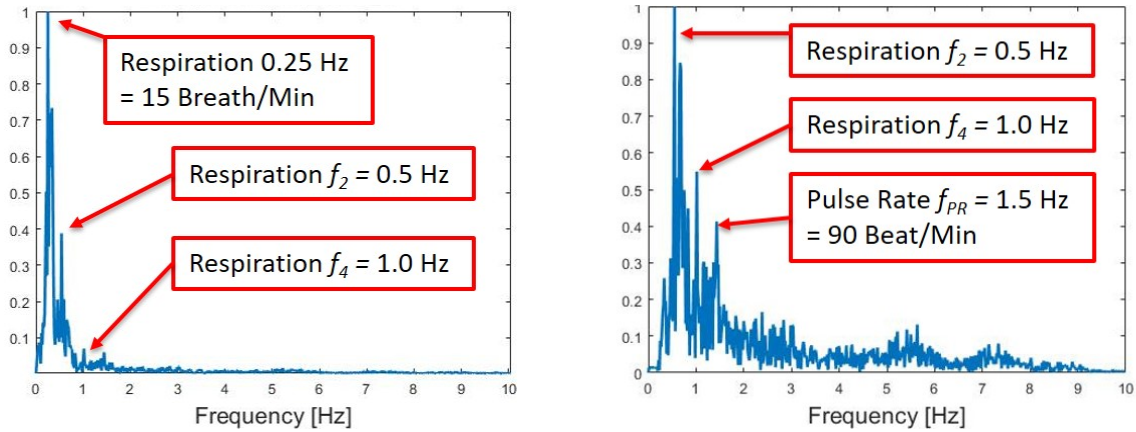


Figure 25. Respiration harmonic mistaken for a pulse rate fundamental harmonic: (left) an unfiltered BCG spectrum that includes a respiration harmonic at 0.25 Hz with harmonics at 0.5 and 1.0 Hz, respectively, and (right) a filtered spectrum with the fundamental respiration harmonic removed.

Strategies proposed to overcome this effect include the removal of the periodic respiration harmonics, but this method was ultimately discarded due to its potential to remove the fundamental pulse component or other important spectral information. In the example illustrated in Figure 25, the removal of the 0.5 , 0.75 and 1.0 Hz components would result in a more accurate pulse rate estimate. However, situations have arisen such that respiration rate is, e.g., 0.4 Hz while the pulse rate is 1.2 Hz. Applying the respiration-harmonic-removal method would result in the cancellation of the 1.2 Hz peak, causing information loss and incorrect results.

While the film data are also susceptible to mattress oscillations, the heart beat components are relatively strong compared to these oscillations. The load cells are not as vulnerable to mattress spring oscillations compared to the films, but other forms of noise can easily corrupt load cell BCGs, most notably vibrations from the ground resulting from footsteps or door openings/closings.

The Bland-Altman plot in Figure 26 for film-based BCGs reflects the extreme outliers present as a result of respiration harmonics. These result in a wider distribution. Removal of the data affected by the respiration harmonics results in a much more acceptable Bland-Altman plot, as depicted in Figure 27. Without the extreme outliers, the distribution becomes narrower, and the majority of the data points now fall within 3 bpm of the mean. This indicates that solving the respiration harmonic problem is critical to ensuring that the peak-scoring algorithm can be reliably

applied to film-based BCGs to determine pulse rate. The Bland-Altman plot for the load cell-based BCGs in Figure 28 exhibits similarities to the film-based Bland-Altman plot when the effects of the respiration harmonics are lessened. This affirms that the peak-scoring algorithm can be applied to load cell-based BCG spectra.

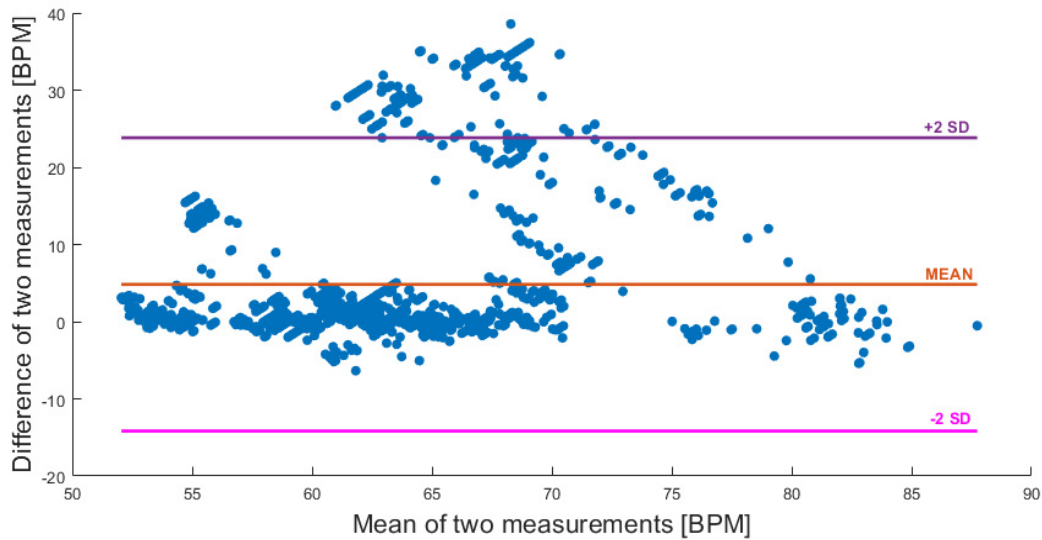


Figure 26. Bland-Altman plot comparing estimated BCG and ECG pulse rates using data acquired with films, where film data are affected by respiration harmonics.

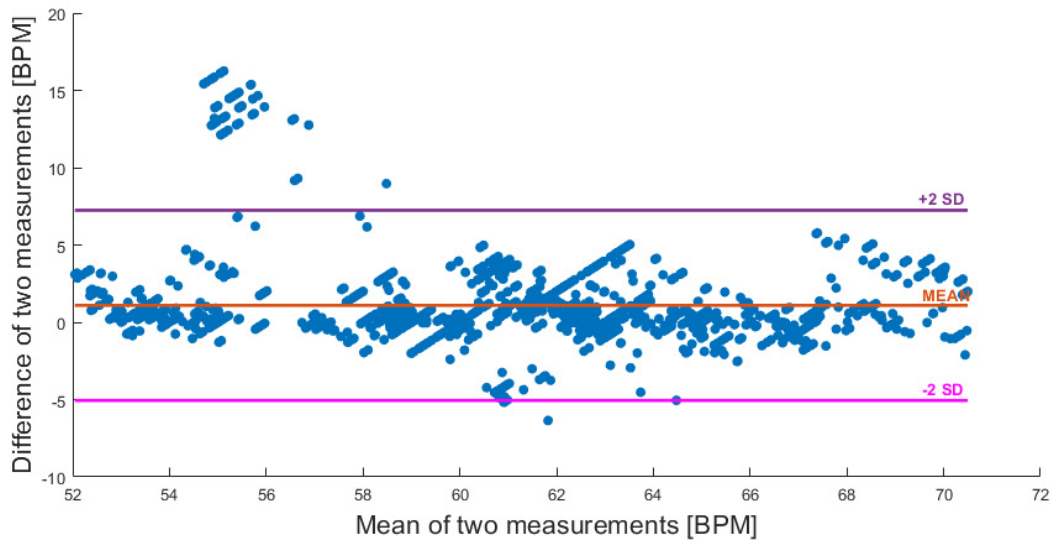


Figure 27. Bland-Altman plot comparing estimated BCG and ECG pulse rates using data acquired with films, where film data are not affected by respiration harmonics.

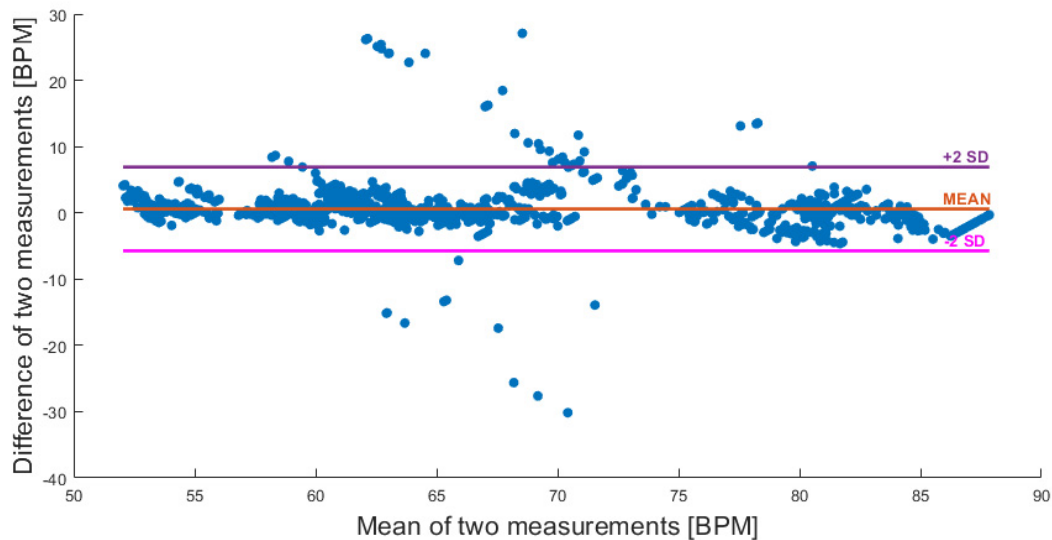


Figure 28. Bland-Altman comparing estimated BCG results and ECG results using data measured from load cells.

6.2.2. Effects of Sleeping Position

During the studies for single-person pulse rate detection, four common sleeping positions were addressed: supine (back), right side, left side, and prone (stomach). Data were acquired for 2 minutes from each of the 5 participants, resulting in a total of 80 two-minute-long segments, or 4,800 data points, for each of the four sleeping positions. Figure 4 illustrated representative BCG waveforms for those sleeping positions, while Figure 12 displayed their corresponding frequency spectra. It comes as no surprise that sleeping position plays an important role in determining the performance of the peak-scoring algorithm. As with previous comparisons, ECG pulse rates were used as ‘true’ values when evaluating estimated pulse rates obtained using the peak-scoring algorithm.

Sleeping position dictates the direction of the propagating forces and creates variations in BCG waveform shapes. As the peak-scoring algorithm operates in the frequency domain, its performance with regard to pulse rate estimation is less susceptible to changes in BCG shape than time-domain peak-detection methods. Table 5 lists the overall errors in pulse rate estimation associated with various sleeping positions, including outliers resulting from respiration. The errors displayed are very similar, with a range of 8.15 to 9.30 bpm.

Table 5. Pulse rate error as a function of sleeping position.

Sleeping Position	RMS Error [BPM]
Supine	9.30
Right Side	8.15
Left Side	9.22
Prone	8.59

The peak-scoring algorithm exhibits consistent results regardless of sleep position, where slightly better performance is obtained when the subject sleeps on their right side, and slightly worse performance is obtained when the subject sleeps in a common supine position. The Bland-Altman plots in Figure 29 to Figure 32 display the performance of the algorithm for each position.

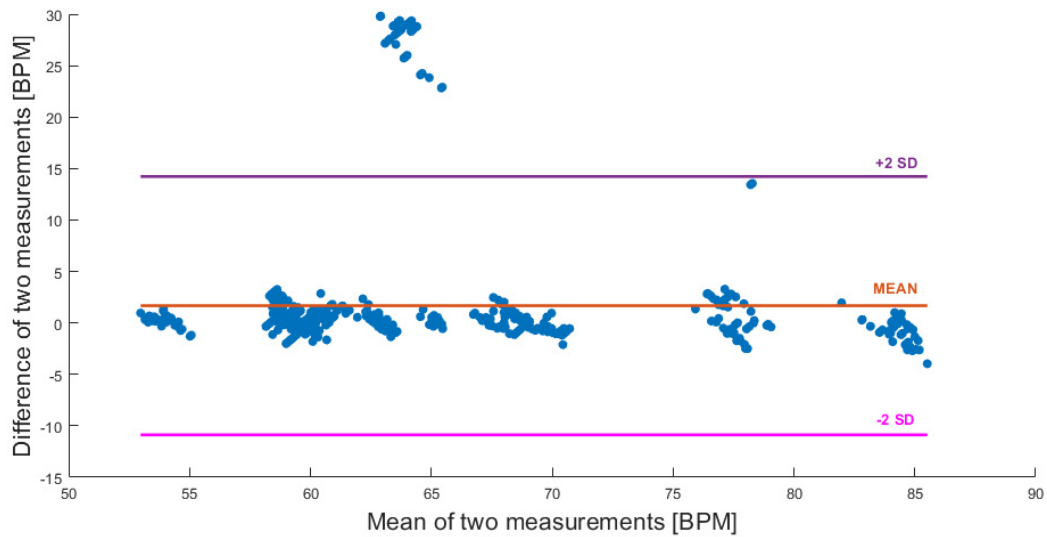


Figure 29. Bland-Altman plot comparing pulse rates estimated from BCGs and ECGs for a single subject sleeping in a supine position.

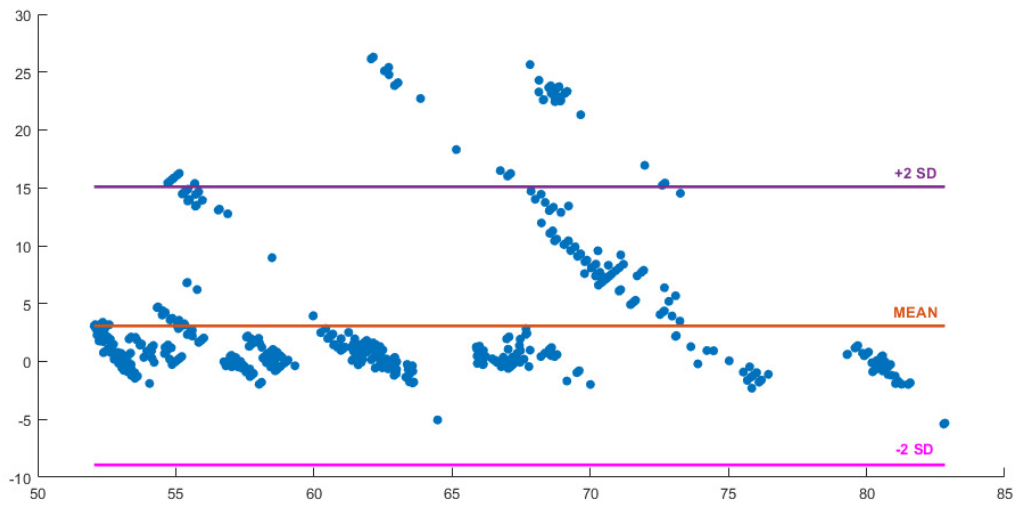


Figure 30. Bland-Altman plot comparing pulse rates estimated from BCGs and ECGs for a single subject sleeping on their right side.

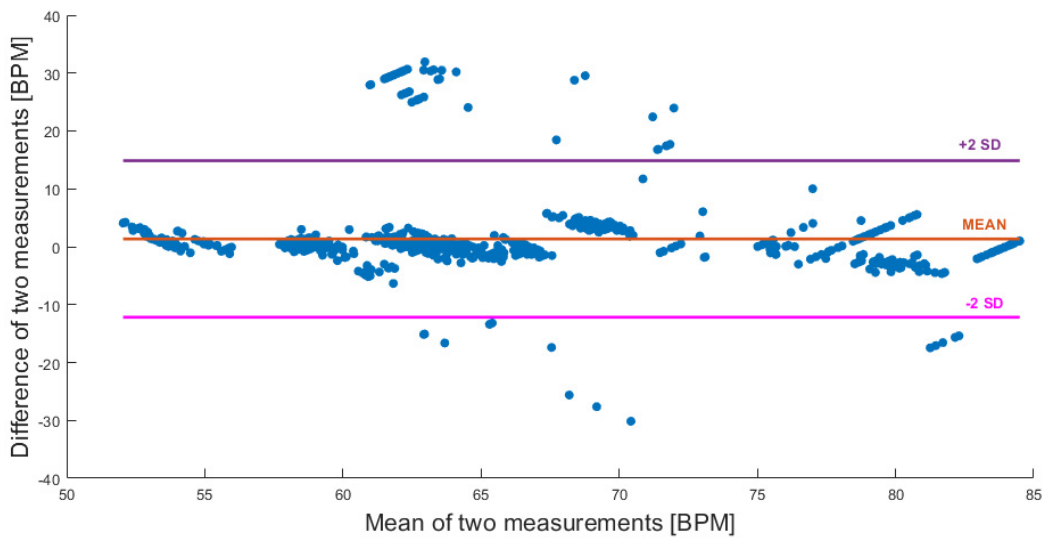


Figure 31. Bland-Altman plot comparing pulse rates estimated from BCGs and ECGs for a single subject sleeping on their left side.

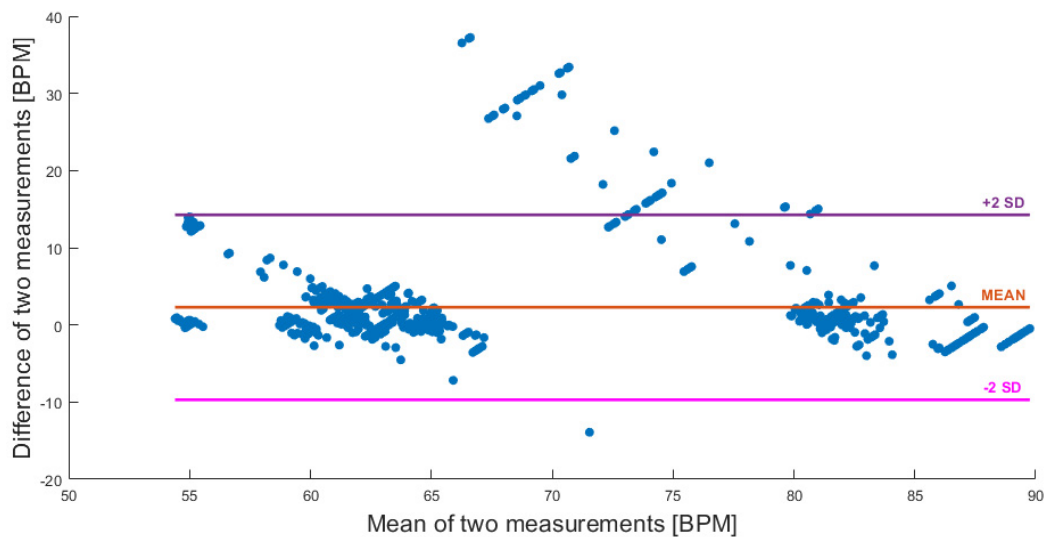


Figure 32. Bland-Altman plot comparing pulse rates estimated from BCGs and ECGs for a single subject sleeping in a prone position.

Of the four positions addressed above, the supine position facilitated the most consistent peak-scoring algorithm performance, with most error values occurring within ± 5 bpm; only extreme outliers were responsible for the high overall error. For the remaining three positions, the algorithm displayed more frequent and inconsistent estimates – not only from extreme outliers – indicating intervals of algorithm failure. The majority of the errors fell within ± 5 bpm, highlighting the algorithm’s ability to function for different sleeping positions and to adapt to variations in BCG waveforms.

6.2.3. Effects of Mattress Type

Mattress type is an important factor because oscillations from mattress springs affect collected BCGs. Both a soft spring mattress and a hard spring mattress were utilized in this study. Data were acquired for 2 minutes from each of the 5 participants, resulting in a total of 160 two-minute-long segments, or 9,600 data points, for each of the two mattress types. The hard spring mattress dampens vibrations, decreasing the effects of mattress oscillations, but the resulting BCGs experience difficulty propagating through the hard mattress to the sensors. The pulse rate errors associated each sensor/mattress combination are listed in Table 6. Bland-Altman plots in Figure 33 and Figure 34 present collective pulse rate errors for the soft and hard mattresses, respectively.

Table 6. RMS pulse rate errors for various mattress/sensor combinations.

Mattress and Sensor Type	RMS Error [BPM]
Soft + Film Only	13.15
Soft + Load Cell Only	1.09
Hard + Film Only	11.56
Hard + Load Cell Only	2.12
Soft + Film and Load Cell	9.33
Hard + Film and Load Cell	8.31

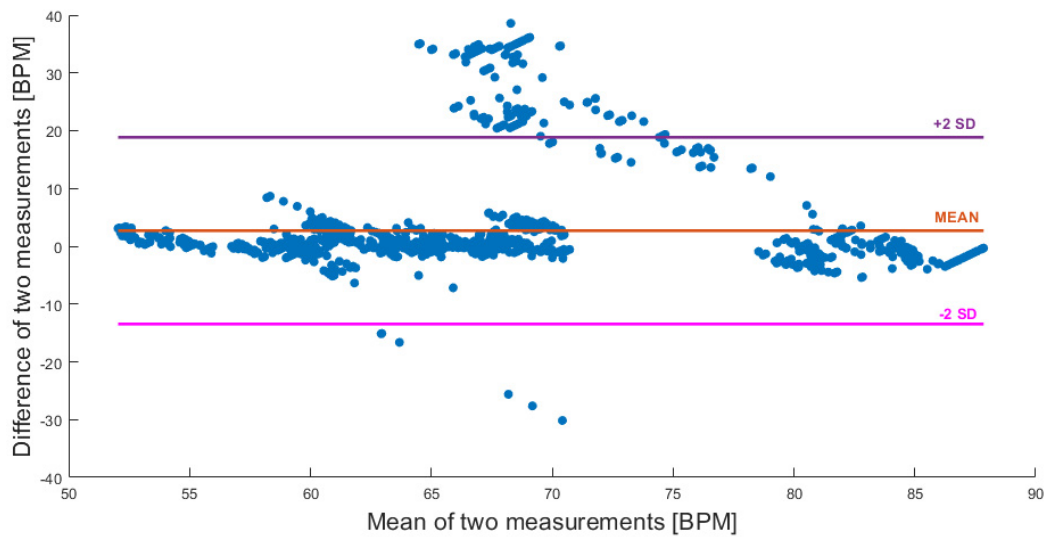


Figure 33. Bland-Altman plot comparing pulse rates estimated from BCGs and ECGs for a single subject sleeping on a soft mattress.

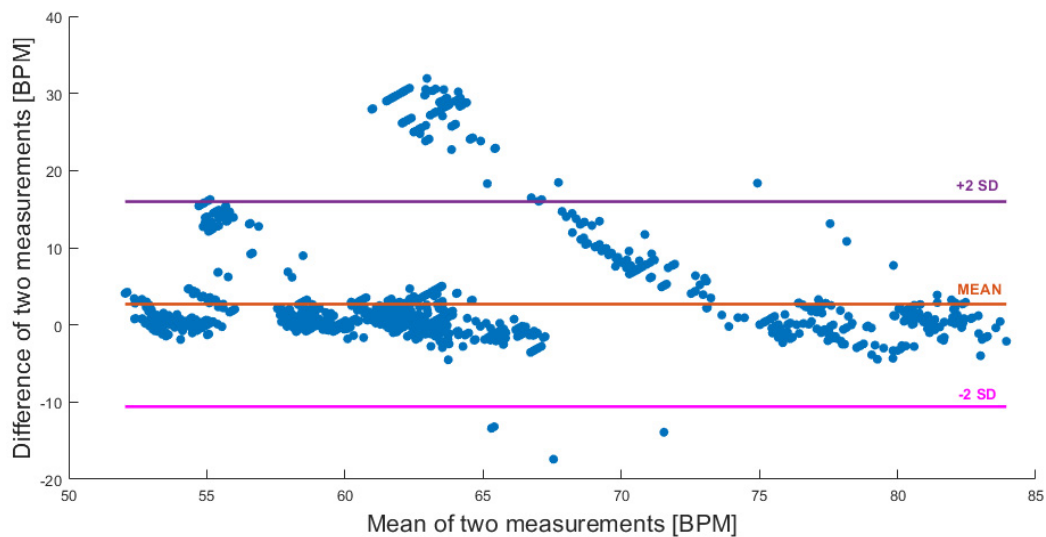


Figure 34. Bland-Altman plot comparing pulse rates estimated from BCGs and ECGs for a single subject sleeping on a hard mattress.

These results indicate that mattress type has a greater impact on algorithm performance when films are used instead of load cells. This is sensible, since a mattress directly couples the film sensors to the body, whereas the bed frame couples the load cells to the mattress and ultimately to the body. The algorithm performs more poorly when films are used in conjunction with the soft mattress instead of the hard mattress. The algorithm performs best when load cells are used in conjunction with the soft mattress (though performance is similar for both mattress types). Overall, the hard mattress led to more consistent algorithm results, though the use of both mattresses led to extreme pulse rate outliers that skewed the distributions.

6.2.4. Effects of Motion Artifact

While each subject was asked to lay still for the duration of the study, minor body movements that create BCG artifacts are inevitable. Given the heightened sensitivity of both the film and load-cell circuitry, even a slight twitch of an arm can cause significant artifact in the BCG recording. However, the signal corruption will often be present only in a single film or load cell BCG, and due to the redundancy in the system, the errant pulse rate provided by that single film or load cell can be identified and discarded as an outlier by the final filter. Motion may be more than a twitch (for example, when the subject sneezes), in which case the associated artifact will be evident on all film and load cell signals. Artifact present in a time-domain BCG will affect the

frequency spectrum, especially when that artifact occupies a greater percentage of the time window. Motion corruption creates extra peaks in the spectrum. These extra peaks, especially peaks with high magnitudes, will be selected first by the peak detection process. If the true fundamental harmonic is weaker and buried within stronger peaks, there is a risk that the true peak will be ignored during the selection process. Figure 35 displays a BCG recording with minor motion artifact that occurs at around 20 seconds. While this artifact seems minor, the resulting false peaks inserted into the spectrum clearly affect the performance of the peak-scoring algorithm.

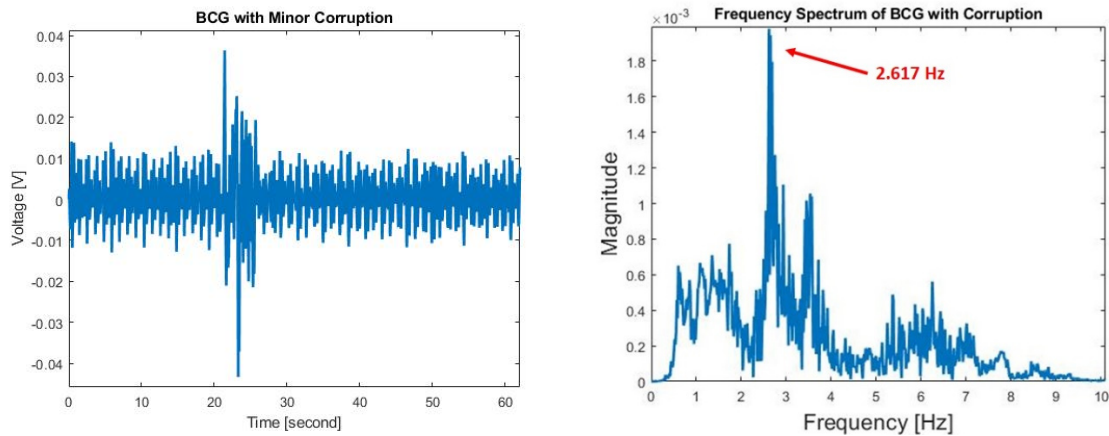


Figure 35. BCG with minor motion artifact (left), which carries over to the frequency spectrum (right).

6.3. Mixed BCGs

Paired (mixed) BCGs were carefully analyzed. Using the MICA decomposition approach described in Chapter 5, each mixed BCG acquired from the films and the load cells was separated into the source signals, s_1 and s_2 . Here, s_1 and s_2 are assumed to be the separated BCGs for each of the two individuals whose data were recorded with each film or load cell, respectively. Each is a matrix of size $4 \times n$, where each of the four rows corresponds to a specific film or load cell (i.e., row 0 through row 3), and n is the number of samples in each recording. Figure 36 displays a mixed signal separated into its two individual component sources. For each mixed BCG, results over two minutes were observed, and outliers were removed using a 5-wide sliding median window. Similar to the earlier studies conducted for a single-person setup, the effects of mattress

type and sensor type were assessed. The differences between the single- and two-person studies were (a) the inclusion of film configurations and (b) the lack of sleeping positions. For the two-step process of separation and pulse rate estimation, it is difficult to assign errors in pulse rate estimates to a specific step.

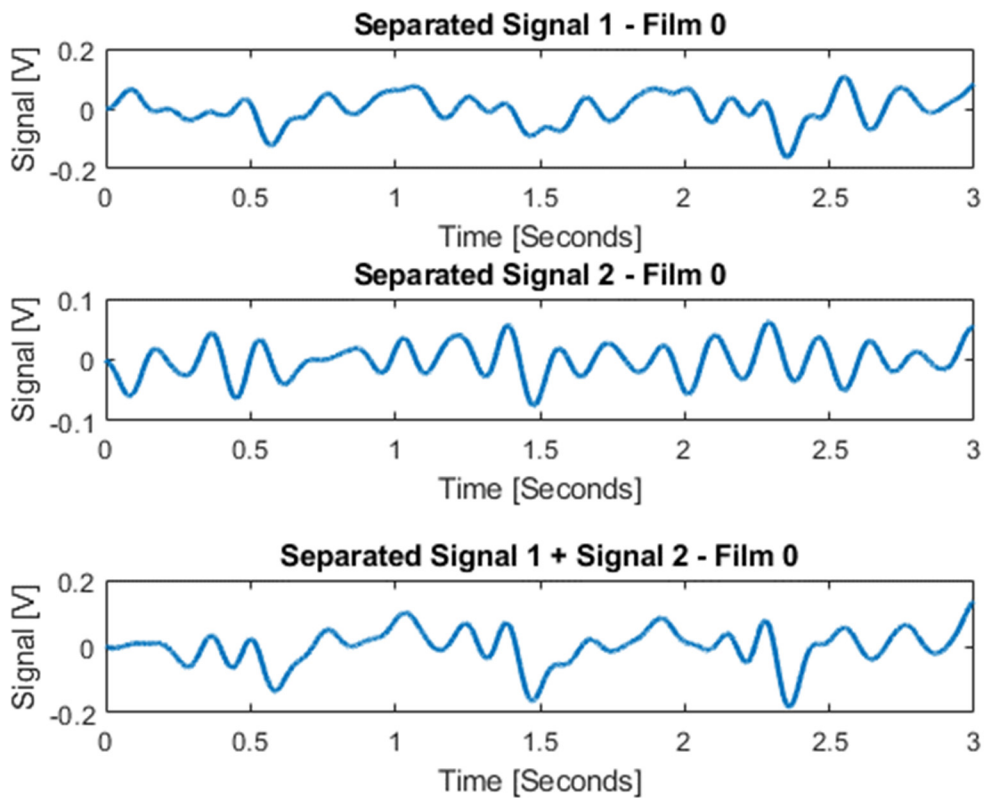


Figure 36. BCG mixture separated into two separate BCGs.

Separated BCGs may lose some of their waveform features as a result of the separation process. This decreases the performance of any peak-detection algorithm which seeks to locate certain time-domain BCG features. Figure 37 illustrates a mixed EMFi BCG signal separated into two source components using MICA decomposition. Each separated BCG does not resemble a typical single-person BCG for a supine position; some features were lost during the separation stage.

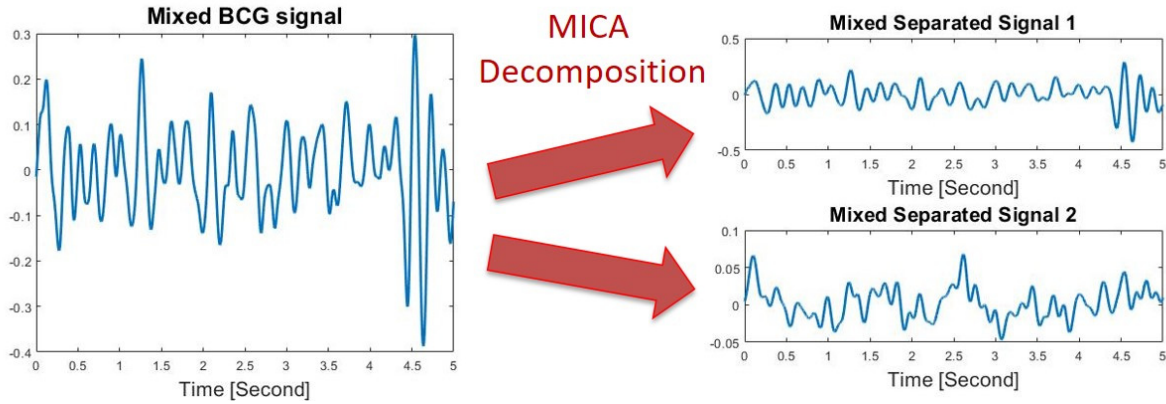


Figure 37. Mixed BCG collected from an EMFi and separated into two BCG source components using MICA decomposition.

6.3.1. Films Versus Load Cells

In an earlier section related to single-person studies, the peak-scoring algorithm demonstrated slightly better performance when applied to load cell BCG spectra as compared to film BCG spectra, although in both cases the algorithm has an acceptable margin of error. Film BCG spectra are vulnerable to mattress vibrations, and the spectral components created by these vibrations can be distinguished from BCG frequency components by the peak-scoring algorithm. However, with two persons on the bed, the effects of the mattress vibrations on the separation method and the resulting scoring process remain to be seen. For the two person study, data were acquired for 2 minutes from each of the 10 participant pairings, resulting in a total of 1520 two-minute-long mixed BCG segments, or 9,120 data points, for each of the eight bed sensors. Table 7 presents the average RMS errors in the pulse rates returned by the peak-scoring algorithm for cases where two individuals lay on the sensor bed at the same time. Film and load cell BCGs were mixed BCGs, meaning they had to be separated prior to pulse rate determination. The full set of values and pulse rates from the study is listed in *Appendix A*. Pulse rate results are skewed by outliers that depend on configuration choices and the presence of respiration harmonics, as noted previously. Pulse rates from BCGs recorded using load cells were unaffected by film configurations and respiration harmonics. Few incorrect pulse rate estimates were present within both the film and load cell datasets when one excludes data affected by configuration or respiration. Possible causes for error include the improper identification of components during MICA decomposition and the incorrect detection of the fundamental peak using the peak-scoring

algorithm. Nonetheless, the algorithm is able to successfully separate signals and extract pulse rate information within an acceptable tolerance. As before, the load cells out-perform the films in terms of providing BCGs that promote correct pulse-rate extraction. A box plot that compares the pulse rate results for the film and load cell sensors is presented in Figure 38, where the load cells lead to the best algorithm performance – a narrower distribution and fewer outliers.

Table 7. RMS errors for pulse rates determined from EMFi and load cell BCGs for the two-subject study.

Sensor Type	RMS Error [BPM]
Film (with Respiration)	7.94
Load Cell	6.80

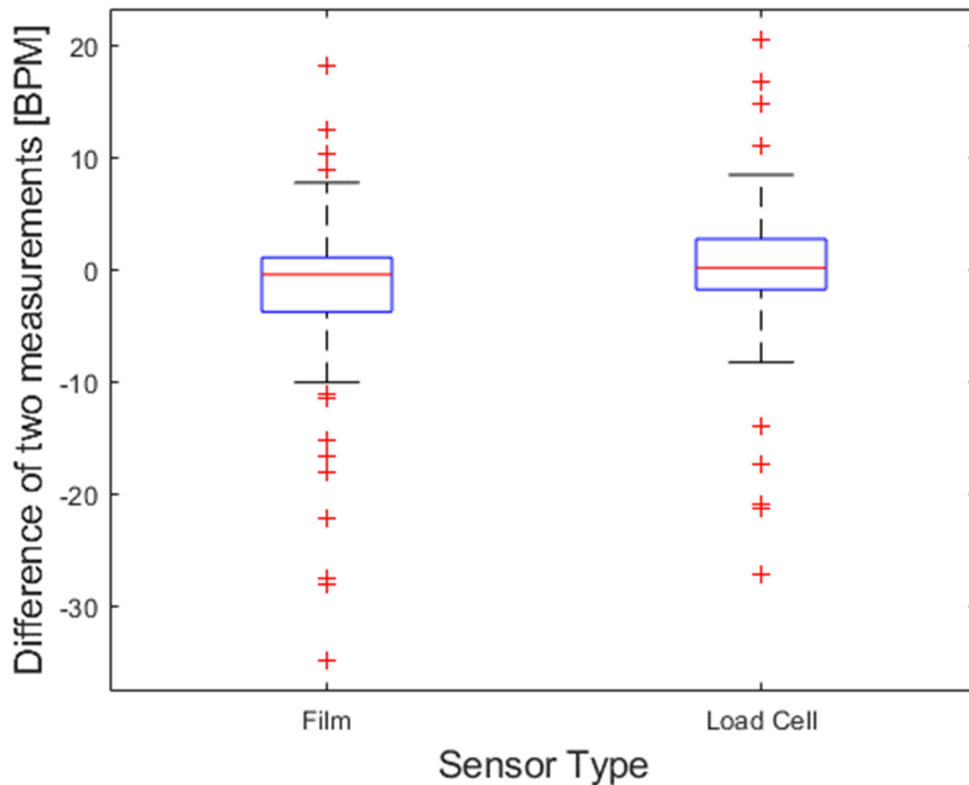


Figure 38. Box-plot for pulse rate comparisons given different sensor types.

6.3.2. Effects of Film Placement

Film placement is an issue that is unique to the two-body problem. Various possible film placement configurations were considered, and the two configurations which displayed the best results during preliminary studies were *Configuration 1* and *Configuration 2* as laid out in Figure 10. Configuration 1 utilizes all four EMFs under one person (subject A), where the associated BCGs will indicate a stronger signal presence for that subject compared to the other subject (subject B). For this configuration, the increased number of sensors may increase accuracy during signal separation. However, the risk is that the BCG received from subject B will not be analyzable due to the intensity of subject A's BCG. Configuration 2, which utilizes two film under each subject, seeks to balance the respective BCG contributions.

For the film configuration data, only mixed BCGs from films were used for the study. Data were acquired for 2 minutes from each of the 10 participant pairings, resulting in a total of 76 two-minute-long segments, or 4,560 data points, for each of the two film placement configurations. Table 8 presents the average RMS errors in the pulse rates returned by the peak-scoring algorithm for each of these two film configurations. Results from the load cells were not included, since the film configurations do not affect load cell data. Full results from this study are tallied in *Appendix A*. Both film configurations suffer from respiration harmonics, but only configuration 1 suffers from the occasional inability to detect subject B's pulse rate from within the mixed BCGs. The box plot in Figure 39 further displays the superiority of configuration 2.

Table 8. RMS errors for pulse rates obtained using different film configurations in the two-person study.

Film Configuration	RMS Error [BPM]
Configuration 1 (All Films Under Subject A)	9.56
Configuration 2 (2 Films Under Each Subject)	7.34

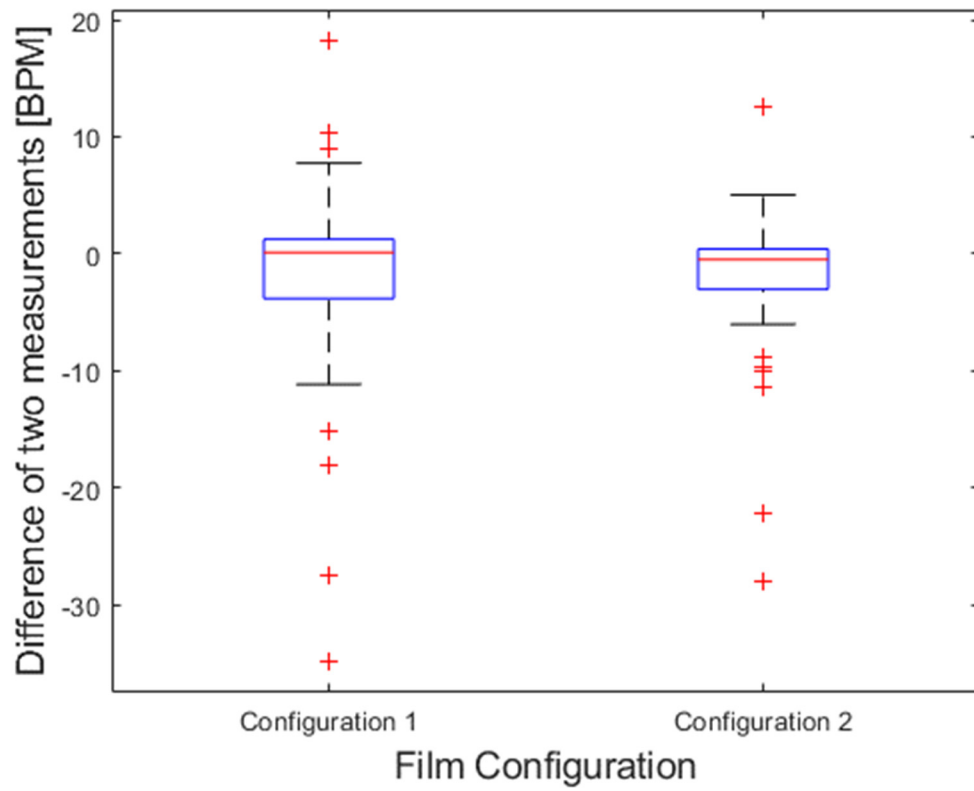


Figure 39. Box plot for pulse rate comparisons given different film configurations.

6.3.3. Effects of Mattress Type

The effects of utilizing a soft spring mattress versus a hard spring mattress were addressed earlier in the chapter when only a single subject was on the sensor bed. The results indicated that the hard spring mattress promoted better overall pulse rate algorithm performance and that mattress type can significantly impact film-based BCG estimates. For the two-person study, data were collected for 2 minutes from each of the 10 participant pairings, resulting in a total of 152 two-minute-long segments, or 9,120 data points, for each of the two mattress types. The effects of the mattress play an additionally important role in terms of source separation. It is vital to minimize mattress vibrations, as any additional signal components caught in the mixed signal make separation more difficult; the algorithm may falsely identify these as source components. The two-subject pulse rate errors affiliated with the use of different mattress types are presented in Table 9.

Table 9. RMS errors for pulse rates obtained from BCGs using different mattress types (two-person study).

Mattress and Sensor Type	RMS Error [BPM]
Soft + Film Only	10.21
Soft + Load Cell Only	8.29
Hard + Film Only	6.24
Hard + Load Cell Only	5.64
Soft + Film and Load Cell	9.30
Hard + Film and Load Cell	5.95

Focusing on film-based BCGs, it is evident that sensor films offer better peak-scoring algorithm performance with the hard spring mattress. This result is consistent with the single-subject studies, but on a larger scale. The oscillations from the soft spring mattress do indeed appear to contribute additional components which the algorithm mistakes as source components during separation. Recall that the algorithm is instructed to search for only two source components: one for each subject. If the algorithm determines a spring component to be one of the two source

components, the algorithm misses the other pulse rate entirely. Figure 40 presents a pulse rate error comparison between the soft and hard mattresses.

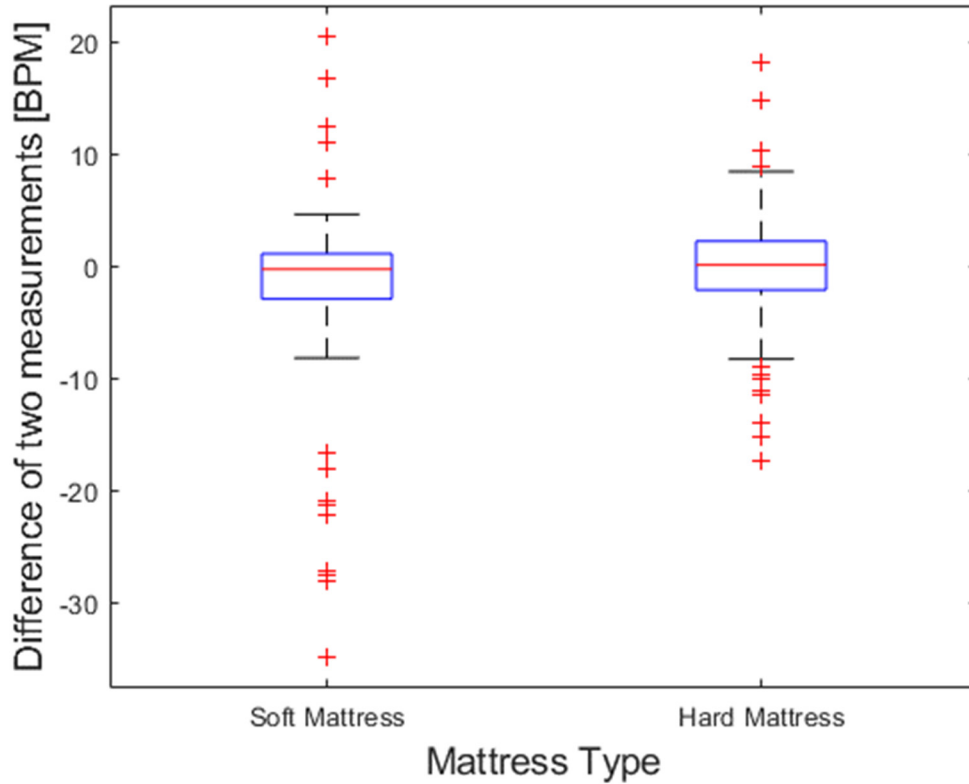


Figure 40. Box plot for pulse rate comparisons given different mattress types.

As is apparent in Figure 40, the soft mattress data contain more outliers, likely resulting from incorrect source separation and the false detection of the fundamental pulse component due to interfering spring components. The hard spring mattress adds the fewest oscillations to the BCGs (i.e., oscillations that affect film-based data more than load cell data), while the soft spring mattress adds more error to the separated signals, but in aggregate the pulse rate estimates remain sufficient for use. An alternative is to remove or dampen the spring oscillations from the BCGs in a preprocessing deconvolution step.

6.4. Performance Summary

The peak-scoring and separation algorithms have achieved acceptable results in terms of identifying pulse rates within an acceptable range of ground truth values measured using a medical-grade patient monitor, even considering moderate variations in the sleep environment. While the system produced acceptable results for all scenarios, certain factors drove better performance. BCGs from load cell sensors produced acceptable pulse-rate-extraction results more frequently than BCGs from film sensors, primarily due to the effects of respiration and spring oscillations on film BCG spectra. This does not mean that load cells are superior to EMFs for sensor bed applications, but for the pulse rate extraction tasks investigated here, the load cell BCGs offered superior results.

Regarding the two-person study, Configuration 2 produced more accurate results than Configuration 1. This outcome was consistent with expectations, since Configuration 2 places two sensors directly below each of the two individuals, reducing the possibility of stronger BCGs burying weaker BCG components. Configuration 1 offers the advantage of a strong signal for the person lying on top of the sensors (Subject A), so configuration 1 is useful in a scenario where only subject A's pulse rate is of interest. Note that prior knowledge of subject A's expected pulse rate is still required to extract pulse rate values with confidence.

Evaluations related to the impact of mattress type determined that a harder spring mattress offers the best peak-scoring algorithm performance because of the minimal additional oscillation components introduced into the recorded BCGs. Despite the increased system damping, BCG forces are still able to propagate through the mattress and be recorded successfully by the sensors. While the soft spring mattress introduced more oscillations into the BCGs, the extracted pulse rates still demonstrated acceptable accuracy.

Chapter 7 - Conclusion

A peak-scoring algorithm was implemented to extract pulse rate estimates from BCGs by exploring the frequency domain instead of the time domain. Utilizing the frequency domain avoids issues that plague traditional time-domain, beat-to-beat detection algorithms, including their susceptibility to variations in BCG waveform shapes. The peak-scoring algorithm was applied successfully to BCGs acquired with a variety of common sleeping positions, demonstrating its ability to work properly even in light of changes in BCG waveforms. The algorithm performed successfully with BCG data obtained using two types of bed-based sensors – EMFis and load cells – demonstrating that (a) EMFis and load cells are both viable sensors for BCG collection and (b) the peak-scoring algorithm works with a wide range of collected BCGs.

For the source separation process, the MICA decomposition method was used due to the knowledge that the individual BCG sources are not independent. The separation process was verified by comparing the outputs of the peak-scoring algorithm with pulse rates obtained from commercial equipment. Since it is difficult to obtain single-person BCGs and mixed BCGs simultaneously, only pulse rates were observed. The separation process showed early success in different scenarios, such as during the use of different mattress types and different film layouts.

In conclusion, the overall signal separation and pulse rate extraction process is feasible and could have a significant impact on at-home sleep quality monitoring for people who share a bed at night. While analyzing the frequency spectrum requires a certain delay, making this system unsuitable for some clinical settings, a delay of minutes is not an issue for at-home sleep monitoring applications. Further work remains to improve the precision of the system and to eliminate the undesired influence of respiration harmonics in the frequency domain.

7.1. Future Work

While the separation and peak-scoring algorithms were successful in extracting pulse rate information from two individuals that shared a sensor bed in a controlled environment, improvements to the overall system remain before it is ready for extended application. First, the interference of respiration harmonics with pulse harmonics remains to be resolved. This situation was observed in one of the two subjects in 10% of all film BCGs recorded. Further, it is evident

that a hard spring mattress performs better due to the absence of strong spring oscillations. While soft spring mattresses are viable for obtaining BCGs, removal of the mattress spring components from BCGs will allow for more accurate source separation and pulse rate determination processes.

For full sleep quality monitoring, respiration rate is an important parameter which cannot be ignored. While the algorithm does not extract the respiration rate directly, e.g., as part of the pre-processing filter used in the separation algorithm, this information could be sensibly extracted prior to filtering. The MICA decomposition's ability to separate unfiltered signals remains to be seen, but separation of mixed respiration rates is also critical for health monitoring.

Lastly, since the MICA decomposition does not identify the subject to whom each extracted pulse rate belongs, it is difficult to affirm that the correct pulse rates have been determined for each individual unless corroborating measurements are available. Some thoughts include running a training session on one individual to obtain a 'training signal' to use for comparison later on, or perhaps exploiting delays and phase changes in the signals to determine which subject is lying on top of which sensors.

References

- [1] Handbook of Clinical Neurology, vol. 98, 2011, page vii.
- [2] C. Carlson, A. Suliman, P. Prakash, D. Thompson, S. Wang, B. Natarajan and S. Warren. "Bed-based instrumentation for unobtrusive sleep quality assessment in severely disabled autistic children," *38th Annual International Conference of the IEEE Engineering in Medicine and Biology Society*, Orlando, FL, 2016, pp. 4909–4912.
- [3] O. T. Inan *et al.* "Ballistocardiography and Seismocardiography: A Review of Recent Advances," *IEEE Journal of Biomedical and Health Informatics*, vol. 19, no. 4, pp. 1414–1427, July 2015.
- [4] T. Watanabe and K. Watanabe. "Noncontact method for sleep stage estimation," *IEEE Transactions on Biomedical Engineering*, vol. 51, no. 10, pp. 1735–1748, Oct. 2004.
- [5] A. Vehkaoja, S. Rajala, P. Kumpulainen and J. Lekkala. "Correlation approach for the detection of the heartbeat intervals using force sensors placed under the bed posts," *Journal of Medical Engineering & Technology*, vol. 37, no. 5, pp. 327–333, 2013.
- [6] B.H. Choi, G.S. Chung, J.S. Lee, D.U. Jeong, and K.S. Park. "Slow-wave sleep estimation on a load-cell-installed bed: a non-constrained method," *2009 Institute of Physics and Engineering in Medicine, Physiological Measurement*, vol. 30, no. 11, pp. 1163–1170, 2009.
- [7] Y. Ozgur and S. Rickard. "Blind Separation of Speech Mixtures via Time-Frequency Masking," *IEEE Transactions on Signal Processing*, vol. 52, no. 7, pp. 1830–1847, July 2004.
- [8] A. Belcouchrani, K. Abed-Meraim, and JF Cardoso. "A Blind Source Separation Technique Using Second-Order Statistics," *IEEE Transactions on Signal Processing*, vol. 45, no. 2, pp. 434–444, February 1997.
- [9] P. Comon. "Independent Component Analysis, A new Concept?," *Signal Processing*, vol. 36, Issue 3, April 1994, pp. 287–314.
- [10] J. Pan and W. Tompkins. "A Real-Time QRS Detection Algorithm," *IEEE Transactions on Biomedical Engineering*, vol. BME-32, no. 3, pp. 230–236, March 1985.
- [11] C. Bruser, S. Winter, and S. Leonhardt. "Robust Inter-beat Interval Estimation in Cardiac Vibration Signals," *Physiological Measurement*, Institute of Physics and Engineering in Medicine, vol. 34, no. 2, pp. 123–138, January 23, 2013.

- [12] F.J. Theis, A. Meyer-Base, and E.W. Lang. “Second Order Blind Source Separation Based on Multi-Dimensional Autocovariances,” *Independent Component Analysis and Blind Signal Separation*, vol. 3195, 2004, pp. 726–733.
- [13] JF. Cardoso. “Multidimensional independent Component Analysis,” Proceedings of the 1998 IEEE International Conference on Acoustics, Speech and Signal Processing, Seattle, WA, 1998, vol.4, pp. 1941–1944.
- [14] D. Farina, C. Fevotte, C. Doncarli and R. Merletti, “Blind Separation of linear instantaneous mixtures of nonstationary surface myoelectric signals,” *IEEE Transactions of Biomedical Engineering*, vol. 51, no. 9, pp. 1555–1567, Aug. 2004.
- [15] J. W. Gordon. “Certain Molar Movements of the Human Body Produced by the Circulation of the Blood,” *J. Anat. and Physiol*, vol.11, no. 3, pp. 533–536, 1877.
- [16] C. Carlson, A. Suliman, A. Alivar, P. Prakash, D. Thompson, B. Natarajan and S. Warren. “A Pilot study of an unobtrusive bed-based sleep quality monitor for severely disabled autistic children,” *40th Annual International Conference of the IEEE EMBS*, July 2018, Honolulu, HI, USA, pp. 4343–4346.
- [17] H. Traunmuller and A. Eriksson. “The Frequency Range of the Voice Fundamentals in the Speech of Male and Female Adults,” *Institutionen för lingvistik, Stockholms universitet, S-106 91 Stockholm, Sweden*, 1995.
- [18] J. L. Martin and A. D. Hakim. “Wrist actigraphy,” *Chest*, vol. 139, no. 6, 2011, pp. 1514–1527.
- [19] J.L. Lacoume. “A Survey of Source Separation,” *Proc. First International Conference on Independent Component Analysis and Blind Source Separation ICA’99*, Aussois, France, Jan. 11–15, 1999, pp. 1–6.
- [20] O.T. Inan, M. Etemadi, R.M. Wiard, G.T.A. Kovacs and L. Giovangrandi. “Novel methods for estimating the ballistocardiogram signal using a simultaneously acquired electrocardiogram,” *Proc. IEEE Annu. Int. Conf. Eng. Med. Biol. Soc.*, 2009, pp. 5334–5347.
- [21] B.H. Choi, G.S. Chung, J.S. Lee, D.U. Jeong and K.S. Park. “Slow-wave sleep estimation on a load-cell-installed bed: a non-constrained method,” *Physiol. Meas.*, vol. 30, pp. 1163–1170, 2009.
- [22] J.H. Shin, B.H. Choi, Y.G. Lim, D.U. Jeong and K.S. Park. “Automatic Ballistocardiogram (BCG) beat detection using a template matching approach,” *30th Annual Int. Conference of the Engineering in Medicine and Biology Society (EMBC 2008)*, Vancouver, Canada, pp. 1144–1146, 2008.

- [23] J.M. Kortelainen, M.O. Mendez, A.M. Bianchi, M. Matteucci and S. Cerutti. “Sleep staging based on Signals Acquired Through Bed Sensor,” *IEEE Transactions on Information Technology in Biomedicine*, vol. 14, no. 3, pp. 776–785, May 2010.
- [24] Y. Zhu, H. Zhang, M. Jayachandran, A.K. Ng, J. Biswas and Z. Chen. “Ballistocardiography with fiber optic sensor in headrest position: a feasibility study and a new processing algorithm,” *35th Annual Int. Conference of the IEEE EMBS*, Osaka, Japan, July 2013, pp. 5203–5206.
- [25] S. Rajala and J. Lekkala, “PVDF and EMFi sensor materials – A comparative study,” *Procedia Engineering*, vol. 5, pp. 862–865, 2010.
- [26] Fitbit, <https://www.fitbit.com>.
- [27] Oura Ring, <https://ouraring.com/>.
- [28] Polar, <https://www.polar.com/us-en>.
- [29] F. Adib, H. Mao, Z. Kabelac, D. Katabi and R.C. Miller, “Smart Homes that Monitor Breathing and Heart Rate,” *Proceedings of the 33rd Annual ACM Conference on Human Factors in Computing Systems*, Seoul, Republic of Korea, April 2015, pp. 837–846.
- [30] L. De Lathauwer, B. De Moor and J. Vandewalle. “Fetal Electrocardiogram Extraction by Blind Source Subspace Separation,” *IEEE Transactions on Biomedical Engineering*, vol 47, no. 5, May 2000, pp. 567–572.
- [31] K.V.K. Ananthang and J.S. Sahambi. “Investigation of Blind Source Separation methods for Extraction of Fetal ECG”, *Canadian Conference on Electrical and Computer Engineering*, vol. 4, 2003, pp. 2021–2024.
- [32] A. Suliman, C. Carlson, S. Warren and D. Thompson. “Performance Evaluation of Processing Methods for Ballistocardiogram Peak Detection”, *40th Annual International Conference of the IEEE EMBS*, July 2018, Honolulu, HI, USA, pp. 502–505.
- [33] J.J. Jin, X. Wang, S. Li and Y. Wu. “A Novel Heart Rate Detection Algorithm in Ballistocardiogram Based on Wavelet Transform,” *Second International Workshop on Knowledge Discovery and Data Mining*, 2009, pp. 76–79.
- [34] Z. Chaozhu, L. Siyao and A.K. Abdullah. “A New Blind Source Separation Method to Remove Artifact in EEG Signals”, *Third International Conference on Instrumentation, Measurement, Computer, Communication and Control*, Sept. 2013, Shenyang, China, pp. 1430–1433.
- [35] S. Kaestle, H. Block and M. Block. “Method and Apparatus for Determining the Concentration of a Component”, U.S. Patent 6,122,535, Sept. 19, 2000.

- [36] F. Theis. “Multidimensional Independent Component Analysis Using Characteristic Functions,” *13th European Signal Processing Conference*, 2005, pp 1– 4.
- [37] F. Theis. “Blind Signal Separation into Groups of Dependent Signals Using Joint Block Diagonalization,” *IEEE International Symposium on Circuits and Systems*, Kobe, vol. 6, 2005, pp. 5878–5881.
- [38] J.F. Cardoso and A. Souloumiac. “Blind beamforming for non-Gaussian signals,” *IEE Proceedings –F*, vol. 140, Dec. 1993, pp. 362–370.
- [39] A. Hyvarinen, J. Karhunen, and E. Oja. “*Independent Component Analysis*,” Wiley, New York, 2001.
- [40] I. Starr , A.J. Rawson, H.A. Schroeder and N.R. Joseph. “Studies on the estimation of the Cardiac output in man, and of abnormalities in cardiac function, from the heart’s recoil and the blood’s impacts; the ballistocardiogram,” *American Journal of Physiology*, 1939, Vol. 127, pp. 1–28.
- [41] A. Sahroni, H. Setiawan and E. Marfianti. “Performance of Blind Source Separation (BSS) Techniques for Mixed Source Signals of EEG, ECG and Voice Signals,” *IEEE 7th International Workshop on Computational Intelligence and Applications*, Nov. 2014, Hiroshima, Japan, 2014, pp. 213–217.
- [42] J.F. Cardoso and A. Souloumiac. “Blind beamforming for non-Gaussian signals,” *IEE proceedings-F*, vol. 140, no. 6, pp. 362–370, Dec. 1993.
- [43] D.N. Rutledge and D.J. Bouversse. “Independent Component Analysis with JADE algorithm,” *TrAC Trends in Analytical Chemistry*, vol. 67, April 2015, pp 22–32.
- [44] K.S. Park, S.H. Hwang, D.W. Jung, H.N. Yoon and W.Y. Lee. “Ballistocardiography for noninvasive sleep structure estimation,” *36th Annual International Conference of the IEEE EMBS*, 2014, Chicago, IL, USA, pp. 5184–5187.
- [45] O.T. Inan, D. Park, L. Giovangrandi and G.T.A. Kovacs. “Noninvasive Measurement of Physiological Signals on a Modified Home Bathroom Scale,” *IEEE Transactions on Biomedical Engineering*, vol. 59, no. 8, Aug. 2012, pp. 2137–2143.
- [46] J.M. Bland and D.G. Altman. “Statistical Methods for Assessing Agreement between Two Methods of Clinical Measurements,” *The Lancet*, Feb. 1986, vol. 327, no. 8476, pp. 307–310.
- [47] E.R. Laskowski, “What’s a normal resting heart rate?,” <https://www.mayoclinic.org/healthy-lifestyle/fitness/expert-answers/heart-rate/faq-20057979>.

- [48] A. Suliman, C. Carlson, C. Ade, S. Warren and D. Thompson “Performance Comparison for Ballistcardiogram Peak Detection Methods,” *IEEE Access*, vol. 7, pp. 53945-53955, April 2019.
- [49] Beddit [<https://www.beddit.com>]
- [50] Emfit [<https://www.emfit.com>]
- [51] M.H. Bonnet and D.L. Arand. “Heart Rate Variability: Sleep Stage, Time of Night and Arousal Influences,” *Electroencephalogr. Clin. Neurophysiol.*, vol. 102, no. 5, pp. 390–396, May 1997.
- [52] D. Young. “Self-measure of Heart Rate Variability (HRV) and Arrhythmia to monitor and to manage atrial arrhythmia: Personal experience with high intensity interval exercise (HIIE) for the conversion to sinus rhythm,” *Frontiers in Physiology*, Vol. 5, 2014, pp. 1–4.
- [53] Arrhythmia, <https://www.nhlbi.nih.gov/health-topics/arrhythmia>.
- [54] W.K. Lee, H. Yoon, C. Han, K.M. Joo and K.S. Park. “Physiological Signal Monitoring Bed for Infants Based on Load-Cell Sensors,” *Sensors*, vol. 16, no. 3, p. (409)1-19, 2016.
- [55] K. Lydon, B.Y. Su, L. Rosales, M. Enayati, K.C. Ho, M. Rantz and M. Skubic. “Robust Heartbeat Detection from In-Home Ballistocardiogram Signals of Older Adults Using a Bed Sensor,” *37th Annual International Conference of the IEEE Engineering in Medicine and Biology Society*, 2015, pp. 7175–7179.

Appendix A - Separation Data Results

Heart rate comparisons between the peak-scoring algorithm and the ground truth method(s).

Table 10. Pulse rate comparison: single subject, soft mattress, film sensors

	Supine position			Right side position		
Subject	Est. PR (BPM)	True PR (BPM)	Difference (BPM)	Est. PR (BPM)	True PR (BPM)	Difference (BPM)
A	59.9124	60.216	-0.3036	52.5808	54.0029	-1.4221
B	60.182	59.7918	0.3902	57.4239	57.0768	0.3471
C	64.9837	65.2382	-0.2545	62.5982	62.2746	0.3236
D	68.8085	68.7841	0.0244	66.86	67.2669	-0.4069
E	52.4547	83.9934	-31.5387*	55.6086	80.3122	-24.7036*
	Left side position			Prone position		
Subject	Est. PR (BPM)	True PR (BPM)	Difference (BPM)	Est. PR (BPM)	True PR (BPM)	Difference (BPM)
A	54.7015	55.4853	-0.7838	59.4492	59.442	0.0072
B	63.255	58.8855	4.3695	58.8283	62.5457	-3.7174
C	63.4769	63.9148	-0.4379	65.1525	64.8273	0.3252
D	61.0977	69.1641	-8.0664	64.6484	65.1766	-0.5282
E	55.2857	78.6978	-23.4121*	49.6085	84.2825	-34.674*

* Respiration harmonic effect

Table 11. Pulse rate comparison: single subject, soft mattress, load cell sensors

	Supine position			Right side position		
Subject	Est. PR (BPM)	True PR (BPM)	Difference (BPM)	Est. PR (BPM)	True PR (BPM)	Difference (BPM)
A	59.1959	60.216	-1.0201	53.1903	54.0029	-0.8126
B	59.8977	59.7918	0.1059	57.2188	57.0768	0.142
C	65.1127	65.2382	-0.1255	61.989	62.2746	-0.2856
D	68.7505	68.7841	-0.0336	66.8763	67.2669	-0.3906
E	84.0917	83.9934	0.0983	80.5166	80.3122	0.2044
	Left side position			Prone position		
Subject	Est. PR (BPM)	True PR (BPM)	Difference (BPM)	Est. PR (BPM)	True PR (BPM)	Difference (BPM)
A	55.6816	55.4853	0.1963	59.2815	59.442	-0.1605
B	58.81	58.8855	-0.0755	59.5234	62.5457	-3.0223
C	63.7024	63.9148	-0.2124	64.8298	64.8273	0.0025
D	67.2067	69.1641	-1.9574	64.8894	65.1766	-0.2872
E	81.647	78.6978	2.9492	83.9699	84.2825	-0.3126

Table 12. Pulse rate comparison: single subject, hard mattress, film sensors

	Supine position			Right side position		
Subject	Est. PR (BPM)	True PR (BPM)	Difference (BPM)	Est. PR (BPM)	True PR (BPM)	Difference (BPM)
A	53.5647	53.8387	-0.274	53.5743	54.9692	-1.3949
B	58.5539	59.9907	-1.4368	50.3619	58.6024	-8.2405
C	59.0336	59.168	-0.1344	61.2923	62.3118	-1.0195
D	62.8364	62.8245	0.0119	48.3081	62.7755	-14.4674
E	50.705	77.7356	-27.0306*	55.9499	74.661	-18.7111*
	Left side position			Prone position		
Subject	Est. PR (BPM)	True PR (BPM)	Difference (BPM)	Est. PR (BPM)	True PR (BPM)	Difference (BPM)
A	53.2597	54.0033	-0.7436	54.8311	54.9463	-0.1152
B	58.7874	58.7705	0.0169	61.7804	63.615	-1.8346
C	49.6037	64.0021	-14.3984	57.785	61.7444	-3.9594
D	61.5132	62.2008	-0.6876	63.0996	63.3777	-0.2781
E	47.3082	76.5744	-29.2662*	66.6459	81.7354	-15.0895*

* Respiration harmonic effect

Table 13. Pulse rate comparison: single subject, hard mattress, load cell sensors

	Supine position			Right side position		
Subject	Est. PR (BPM)	True PR (BPM)	Difference (BPM)	Est. PR (BPM)	True PR (BPM)	Difference (BPM)
A	53.51	53.8387	-0.3287	53.5073	54.9692	-1.4619
B	59.6829	59.9907	-0.3078	57.9255	58.6024	-0.6769
C	59.1423	59.168	-0.0257	61.204	62.3118	-1.1078
D	63.2083	62.8245	0.3838	62.3526	62.7755	-0.4229
E	77.118	77.7356	-0.6176	65.6847	74.661	-8.9763
	Left side position			Prone position		
Subject	Est. PR (BPM)	True PR (BPM)	Difference (BPM)	Est. PR (BPM)	True PR (BPM)	Difference (BPM)
A	52.9272	54.0033	-1.0761	54.7013	54.9463	-0.245
B	58.2172	58.7705	-0.5533	63.6547	63.615	0.0397
C	64.9172	64.0021	0.9151	61.8405	61.7444	0.0961
D	62.0681	62.2008	-0.1327	62.7103	63.3777	-0.6674
E	76.267	76.5744	-0.3074	80.4872	81.7354	-1.2482

Table 14. Pulse rate comparison: two subjects, soft mattress, film, config. 1

	Subject A est.	Subject A True	Difference	Subject B Est.	Subject B True	Difference
Data 0	66.1933	65.9705	0.2228	60.6834	58.9992	1.6842
Data 1	63.363	62.2285	1.1345	61.3945	59.6762	1.7183
Data 2	57.0974	58.5382	-1.4408	51.3393*	78.9167	-27.5774
Data 3	81.5806	81.5986	-0.018	63.2989	55.5594	7.7395
Data 4	65.0159	64.2193	0.7966	58.6261	59.4665	-0.8404
Data 5	84.5025	90.186	-5.6835	48.5304*	56.7098	-8.1794
Data 6	75.5237	79.2415	-3.7178	56.7086	57.5233	-0.8147
Data 7	85.3486	89.2553	-3.9067	70.0849	69.0488	1.0361
Data 8	57.2289*	92.0833	-34.8544	71.152	77.0632	-5.9112
Data 9	63.3492^	81.474	-18.1248	60.588	62.1346	-1.5466

* Respiration harmonic effect

^ Configuration effect

Table 15. Pulse rate comparison: two subjects, soft mattress, load cell, config. 1

	Subject A est.	Subject A True	Difference	Subject B Est.	Subject B True	Difference
Data 0	73.7765	65.9705	7.806	58.7975	58.9992	-0.2017
Data 1	61.2777	62.2285	-0.9508	60.779	59.6762	1.1028
Data 2	81.515	78.9167	2.5983	53.6507	58.5382	-4.8875
Data 3	83.5306	81.5986	1.932	56.6241	55.5594	1.0647
Data 4	65.8803	64.2193	1.661	64.09	59.4665	4.6235
Data 5	91.2381	90.186	1.0521	59.624	56.7098	2.9142
Data 6	58.399	79.2415	-20.8425	57.6848	57.5233	0.1615
Data 7	86.4319	89.2553	-2.8234	72.1155	69.0488	3.0667
Data 8	92.192	92.0833	0.1087	74.0794	77.0632	-2.9838
Data 9	77.6767	81.474	-3.7973	60.8563	62.1346	-1.2783

Table 16. Pulse rate comparison: two subjects, soft mattress, film, config. 2

	Subject A est.	Subject A True	Difference	Subject B Est.	Subject B True	Difference
Data 0	62.7415	61.6272	1.1143	55.0119	55.481	-0.4691
Data 1	56.8223	57.9345	-1.1122	51.354	51.7562	-0.4022
Data 2	87.7772	88.8182	-1.041	64.1793	51.6924	12.4869
Data 3	70.9591	76.9828	-6.0237	53.8556	53.4191	0.4365
Data 4	67.424	65.4226	2.0014	58.4567	57.3319	1.1248
Data 5	86.0991	85.697	0.4021	60.1419	57.7586	2.3833
Data 6	55.8516	77.9987	-22.1471	55.7068	57.9174	-2.2106
Data 7	85.6144	88.4904	-2.876	Corrupted PPG		
Data 8	88.4857	88.571	-0.0853	79.1218	74.0911	5.0307
Data 9	66.02063	66.5468	-0.52617	52.1311*	80.1311	-28

* Respiration harmonic effect

Table 17. Pulse rate comparison: two subjects, soft mattress, load cell, config. 2

	Subject A est.	Subject A True	Difference	Subject B Est.	Subject B True	Difference
Data 0	60.311	61.6272	-1.3162	56.685	55.481	1.204
Data 1	55.362	57.9345	-2.5725	52.4696	51.7562	0.7134
Data 2	84.6215	88.8182	-4.1967	68.3472	51.6924	16.6548
Data 3	75.7077	76.9828	-1.2751	53.3946	53.4191	-0.0245
Data 4	70.037	65.4226	4.6144	57.2957	57.3319	-0.0362
Data 5	85.9787	85.697	0.2817	78.2447	57.7586	20.4861
Data 6	56.642	77.9987	-21.3567	55.4696	57.9174	-2.4478
Data 7	87.6144	88.4904	-0.876	Corrupted PPG		
Data 8	89.3043	88.571	0.7333	85.137	74.0911	11.0459
Data 9	66.2272	66.5468	-0.3196	52.9512	80.1311	-27.1799

Table 18. Pulse rate comparison: two subjects, hard mattress, film, config. 1

	Subject A est.	Subject A True	Difference	Subject B Est.	Subject B True	Difference
Data 0	62.1279	60.8896	1.2383	54.8311*	70.065	-15.2339
Data 1	73.1509	72.4836	0.6673	59.3626	70.5323	-11.1697
Data 2	75.3922	74.1463	1.2459	74.6053^	65.6993	8.906
Data 12	65.5024	63.182	2.3204	63.2196^	52.8439	10.3757
Data 13	70.4641	67.3171	3.147	59.6505	55.94	3.7105
Data 14	84.4439	84.0767	0.3672	47.2648	49.8354	-2.5706
Data 15	81.9191	81.332	0.5871	70.7495	70.6141	0.1354
Data 16	66.5802	70.4019	-3.8217	65.809	65.9497	-0.1407
Data 17	85.9875	85.8956	0.0919	85.9183^	67.7084	18.2099

* Respiration harmonic effect

^ Configuration effect

Table 19. Pulse rate comparison: two subjects, hard mattress, load cell, config. 1

	Subject A est.	Subject A True	Difference	Subject B Est.	Subject B True	Difference
Data 0	70.6199	70.065	0.5549	54.8194	60.8896	-6.0702
Data 1	71.7589	72.4836	-0.7247	65.5141	70.5323	-5.0182
Data 2	75.0534	74.1463	0.9071	66.2598	65.6993	0.5605
Data 12	63.3757	63.182	0.1937	53.3195	52.8439	0.4756
Data 13	74.3169	67.3171	6.9998	53.2074	55.94	-2.7326
Data 14	83.8463	84.0767	-0.2304	53.5343	49.8354	3.6989
Data 15	81.0668	81.332	-0.2652	56.6657	70.6141	-13.9484
Data 16	68.3069	70.4019	-2.095	66.1096	65.9497	0.1599
Data 17	83.9508	85.8956	-1.9448	82.5697	67.7084	14.8613

Table 20. Pulse rate comparison: two subjects, hard mattress, film, config. 2

	Subject A est.	Subject A True	Difference	Subject B Est.	Subject B True	Difference
Data 3	63.0399	64.2271	-1.1872	57.6119	58.2732	-0.6613
Data 4	75.2379	74.9553	0.2826	63.2936	63.5735	-0.2799
Data 5	68.5112	70.4437	-1.9325	64.2858	62.1414	2.1444
Data 6	62.0294	65.0586	-3.0292	55.4618	56.2952	-0.8334
Data 7	63.6951	72.5834	-8.8883	53.8606	54.01	-0.1494
Data 8	68.7767*	78.4114	-9.6347	54.2041	54.2796	-0.0755
Data 9	79.6288	91.1081	-11.4793	74.549	74.1617	0.3873
Data 10	66.3947	69.7751	-3.3804	62.3156	65.7989	-3.4833
Data 11	85.9827	81.3002	4.6825	54.9462*	65.0116	-10.0654

* Respiration harmonic effect

Table 21. Pulse rate comparison: two subjects, hard mattress, load cell, config. 2

	Subject A est.	Subject A True	Difference	Subject B Est.	Subject B True	Difference
Data 3	64.7892	64.2271	0.5621	59.5991	58.2732	1.3259
Data 4	77.0639	74.9553	2.1086	67.0025	63.5735	3.429
Data 5	75.8676	70.4437	5.4239	66.6437	62.1414	4.5023
Data 6	67.9093	65.0586	2.8507	55.5252	56.2952	-0.77
Data 7	64.1835	72.4635	-8.28	53.2748	54.01	-0.7352
Data 8	77.6495	78.4114	-0.7619	62.7132	54.2796	8.4336
Data 9	74.0947	91.5027	-17.408	73.1906	74.1617	-0.9711
Data 10	76.2237	69.7751	6.4486	69.3933	65.7989	3.5944
Data 11	79.1574	81.3002	-2.1428	67.7846	65.0116	2.773